Interference, Fluctuation, and Alternation of Electron Tunneling in Protein Media. 2. Non-Condon Theory for the Energy Gap Dependence of Electron Transfer Rate

Hirotaka Nishioka, Akihiro Kimura, and Takahisa Yamato

Department of Physics, Graduate School of Science, Nagoya University, Furo-cho, Chikusa-ku, Nagoya 464-8602, Japan

Tsutomu Kawatsu

Department of Chemistry, Duke University, Durham, North Carolina 27708-0349

Toshiaki Kakitani*

Department of General Education, Faculty of Science and Technology, Meijo University, Tempaku-ku, Nagoya 468-8502, Japan

Received: March 30, 2005; In Final Form: June 15, 2005

Developing the quantum transition rate theory of Prezhdo and Rossky (*J. Chem. Phys.* **1997**, *107*, 5863), we produced a new non-Condon theory of the rate of electron transfer (ET) which happens through a protein medium with conformational fluctuation. The new theory is expressed by a convolution form of the power spectrum for the autocorrelation function of the electronic tunneling matrix element $T_{DA}(t)$ with quantum correction and the ordinary Franck−Condon factor. The new theory satisfies the detailed balance condition for the forward and backward ET rates. The ET rate formula is divided into two terms of elastic and inelastic tunneling mechanisms on the mathematical basis. The present theory is applied to the ET from Bph^- to Q_A in the reaction center of *Rhodobacter sphaeroides*. Numerical calculations of $T_{DA}(t)$ were made by a combined method of molecular dynamics simulations and quantum chemistry calculations. We showed that the normalized autocorrelation function of $T_{DA}(t)$ is almost expressed by exponential forms. The calculated energy gap law of the ET rate is nearly Marcus' parabola in most of the normal region and around the maximum region, but it does not decay substantially in the inverted region, which is called the anomalous inverted region. We also showed that the energy gap law at the high uphill energy gap in the normal region is elevated considerably from the Marcus' parabola, which is called the anomalous normal region. Those anomalous energy gap laws are due to the inelastic tunneling mechanism which works actively at the energy gap far from zero. We presented an empirical formula for easily calculating the non-Condon ET rate, which is usable by many researchers. We provided experimental evidence for the anomalous inverted region which was basically reproduced by the present theory. The present theory was extensively compared with the previous non-Condon theories.

1. Introduction

Electron transfer (ET) reactions in a protein environment play important roles in the high-efficient energy conversion of biological systems.[1] In these ET systems, donor and acceptor cofactors that are bound to protein are separated by long distances (ca. 5−30 Å).[2] Such a long-range electron transfer takes place by the electron tunneling of the superexchange mechanism mediated by the protein environment.[3] The protein environment has minute atomistic structures. It was expected that the electron transfer pathway and the electron transfer rate would be delicately affected by these atomistic structures of the protein.[4−9] In the long-range electron transfer, the electronic coupling between donor and acceptor is weak and the nonadiabatic mechanism works.[10]

The standard expression for such nonadiabatic ET rate is written as

$$k_{DA} = \frac{2\pi}{\hbar}|T_{DA}|^2(\mathrm{FC}) \tag{1}$$

where T_{DA} is the electron tunneling matrix element between the initial state D and the final state A and (FC) is the thermally averaged Franck−Condon factor. In the Condon approximation, T_{DA} is a constant. In the actual situation, the protein conformation fluctuates due to thermal agitation. If the electron tunneling through the protein medium is sensitive to the minute atomistic structure of the protein, T_{DA} would change its value under the fluctuation of protein conformation.[11−18] In the case of slow modulation of T_{DA} as compared with the rapid thermal fluctuation of nuclei constituting the Franck−Condon factor FC, the ET rate is evaluated by the following equation[11,19]

$$k_{DA} = \frac{2\pi}{\hbar}\langle T_{DA}{}^2\rangle(FC) \tag{2}$$

where $\langle\ \rangle$ indicates the statistical average. The electronic factor $\langle T_{DA}{}^2\rangle$ in eq 2 apparently indicates the fact that the protein

* All the correspondence should be addressed to T. Kakitani. Tel: +81-52-838-2394. Fax: +81-52-832-1170. E-mail: kakitani@ccmfs.meijo-u.ac.jp.

10.1021/jp051606i CCC: $30.25
Published on Web 07/23/2005

conformation which gives rise to a large value of T_{DA}^2 contributes to k_{DA} more efficiently.[20] In the special case of the slow modulation where T_{DA}^2 becomes overwhelmingly large in a certain protein conformation, the electron transfer mostly proceeds by waiting for this special conformation of protein. This is the so-called conformational gating.[21,22] The slow modulation of T_{DA} is considered as a kind of non-Condon effect. But its effect is expressed by an ensemble average of only the electronic factor. In the fast modulation of T_{DA}, a more drastic non-Condon effect should appear; a dynamic character of nuclear and electronic coupling emerges. To address this problem, it is desirable to describe the non-Condon effect to the ET rate in all the fluctuation time scales. Then, we can classify the non-Condon effect based on the special property of thermal fluctuation of T_{DA} in a protein environment. From such analysis, we may obtain a picture of elastic and inelastic tunneling mechanisms much more clearly.

Recently, theoretical studies of the T_{DA} fluctuation effects on the ET rate were made by several groups.[23−27] In these studies, the autocorrelation function for the time-dependent T_{DA} was assumed to be a specific function to achieve the analytical ET rate expression. An exponentially decaying autocorrelation function for T_{DA} was used by Tang,[23] by Goychuk et al.,[24] and by Bixon and Jortner.[26] The effect of the T_{DA} fluctuations on the ET rate was discussed as a function of the correlation time τ_c of the autocorrelation function. Especially new aspects of the fast and slow limiting cases for the decay of autocorrelation function were discussed.[23,24] Troisi et al. derived an analytical expression for the ET rate by the perturbation method and by assuming a Gaussian function for the autocorrelation function for T_{DA}.[27] This theoretical model was used to analyze the effects of the T_{DA} fluctuation on the ET rate in a C-clamp molecule by Troisi et al.[28] Stuchebrukhov et al. treated a case of strong dynamic coupling of a tunneling electron with a quantum vibration of the protein media and discussed the effects of inelastic tunneling processes on the free energy gap dependence of the ET rate.[11,25] It should be mentioned here that all these theoretical formulas do not satisfy the detailed balance condition for the forward and backward ET rates. The realistic autocorrelation function of the time-dependent T_{DA} can be obtained by a combined study of molecular dynamics (MD) simulations and quantum chemistry (QC) calculations for each ET system. Such combined studies were made recently in different systems: protein-mediated ET in azurin[19] and solvent-mediated ET in C-clamped molecules.[28] Therefore, it is a possible task to investigate in detail what kind of autocorrelation function is appropriate for the T_{DA} fluctuation in a protein environment.

In the present paper, we make a theoretical formulation for the ET rate, by incorporating the non-Condon effect in all the cases of conformation fluctuation and by satisfying the detailed balance condition. We decouple the non-Condon ET rate into the contribution of the inelastic tunneling mechanism and that of the elastic tunneling mechanism based on a mathematical principle. The role of the elastic and inelastic tunneling mechanisms in the free energy gap dependence of the ET rate (called energy gap law) is clarified. The theory is applied to the electron transfer from the bacteriopheophytin anion (Bph^-) to the primary quinone (Q_A) in the bacterial photosynthetic reaction center of *Rhodobacter sphaeroides*. We show that the inelastic mechanism works overwhelmingly in the energy gap far from zero, causing the ET rate to decrease slowly.

The constitution of this paper is as follows: Formulation of a new theory is made in section 2. For this purpose, we develop the theory for the quantum transition rate by Nitzan et al.[29,30] and Rossky et al.[31,32] to apply to the energy gap law of ET. We improve the theory so that the detailed balance condition might be satisfied. In section 3, we describe a method for the MD simulation of the reaction center and for the QC calculation of T_{DA}. In section 4, numerically calculated results of the new energy gap law are shown. In section 5, many kinds of discussions related to the properties of the new energy gap law are made, including the comparison of the present theory with other theories. Possible experimental evidence for the inelastic tunneling effect is also provided. In section 6, we conclude this paper.

2. Theory

In this section, we derive the non-Condon ET rate formula within the framework of the Fermi's golden rule using the notation of our previous study.[15] Under the Born−Oppenheimer approximation, the initial and final vibronic states for the ET are expressed as

$$\Psi_{iu}(\boldsymbol{r},\boldsymbol{R}) = \psi_i(\boldsymbol{r},\boldsymbol{R})\chi_{iu}(\boldsymbol{R}) \tag{3}$$

$$\Psi_{fv}(\boldsymbol{r},\boldsymbol{R}) = \psi_f(\boldsymbol{r},\boldsymbol{R})\chi_{fv}(\boldsymbol{R}) \tag{4}$$

where $\Psi_{iu}(\boldsymbol{r},\boldsymbol{R})$ and $\Psi_{fv}(\boldsymbol{r},\boldsymbol{R})$ are the initial and final vibronic wave functions, respectively. The coordinates $\boldsymbol{r}$ and $\boldsymbol{R}$ are for electrons and nuclei, respectively. $\psi_i(\boldsymbol{r},\boldsymbol{R})$ and $\psi_f(\boldsymbol{r},\boldsymbol{R})$ are the electronic wave functions in the initial and final states, and $\chi_{iu}(\boldsymbol{R})$ and $\chi_{fv}(\boldsymbol{R})$ are the vibrational wave functions for donor, acceptor, and the protein environment in the vibronic states iu and fv, respectively. The long-range ET rate from donor D to acceptor A is written as

$$k_{DA} = \frac{2\pi}{\hbar}\langle\sum_{v} |\langle\Psi_{iu}(\boldsymbol{r},\boldsymbol{R})|\hat{T}^{DA}|\Psi_{fv}(\boldsymbol{r},\boldsymbol{R})\rangle_{\boldsymbol{r},\boldsymbol{R}}|^2\delta(E_{iu} - E_{fv})\rangle_T \tag{5}$$

where $\hat{T}^{DA}$ is the electron tunneling operator. E_{iu} and E_{fv} are the energies of the vibronic states iu and fv. The brackets $\langle\ \rangle_{\boldsymbol{r},\boldsymbol{R}}$ and $\langle\ \rangle_T$ indicate the integral over $\boldsymbol{r}$ and $\boldsymbol{R}$ and the thermal average over the initial vibrational state u, respectively. Taking the Fourier transformation of the δ-function in eq 5, we obtain the rate formula in the time domain

$$k_{DA} = \frac{1}{\hbar^2}\langle\int_{-\infty}^{\infty} dt\, \langle\chi_{iu}(\boldsymbol{R})|e^{iH_i t/\hbar}T_{DA}(\boldsymbol{R})e^{-iH_f t/\hbar}T_{AD}(\boldsymbol{R})|\chi_{iu}(\boldsymbol{R})\rangle_{\boldsymbol{R}}\rangle_T \tag{6}$$

where

$$T_{DA}(\boldsymbol{R}) = \langle\psi_i(\boldsymbol{r},\boldsymbol{R})|\hat{T}^{DA}|\psi_f(\boldsymbol{r},\boldsymbol{R})\rangle_{\boldsymbol{r}} \tag{7}$$

The operators H_i and H_f are vibrational Hamiltonians corresponding to the electronic states i and f, respectively.

Equation 6 is a quantum rate formula within the Born−Oppenheimer approximation. It is almost impossible to treat vibrations with a full quantum-mechanical theory for the long-range electron transfer. Then, we adopt the frozen Gaussian model[33−35] for the nuclear motion affecting the electronic state to give rise to the time-dependent $T_{DA}(t)$. For the time being, we follow the method of the group of Nitzan[29,30] and the group of Rossky.[31,32] The overlap of the nuclear wave functions propagating on the initial and final potential energy surface is calculated by the frozen Gaussian model. The motion of the center of frozen Gaussian wave functions is described by the classical trajectory of MD simulation. This approximation is

good for the short time of vibrational wave packet propagation. Then, eq 6 can be rewritten as[32]

$$k_{DA} = \frac{1}{\hbar^2}\langle \int_{-\infty}^{\infty} dt\, T_{DA}^{q-c}(t) T_{AD}^{q-c}(0) J(t)\rangle_T \quad (8)$$

where $J(t)$ is the overlap of the two nuclear wave functions that have the same initial functional forms and propagate on the initial diabatic surface and the final diabatic surface, respectively

$$J(t) = \langle \chi_{iu}(\boldsymbol{R}) | e^{iH_i t/\hbar} e^{-iH_f t/\hbar} | \chi_{iu}(\boldsymbol{R})\rangle_{\boldsymbol{R}} \quad (9)$$

and $T_{DA}^{q-c}(t)$ is the time-dependent quantum-classical electronic tunneling matrix element evaluated along the classical nuclear trajectory on the initial diabatic surface

$$T_{DA}^{q-c}(t) = e^{iH_i t/\hbar}\, T_{DA}^{q-c}(0)\, e^{-iH_i t/\hbar} \quad (10)$$

Applying the frozen Gaussian model for the propagation of the vibrational wave packet, Prezhdo and Rossky[32] have shown that $J(t)$ is expressed as

$$J(t) = D(t) \exp\left[\frac{i}{\hbar} \Delta E_{if}(t) t\right] \quad (11)$$

where $D(t)$ is the Fourier transform of the Franck−Condon factor and $\Delta E_{if}(t)$ represents the energy difference $(E_i(\boldsymbol{R}) - E_f(\boldsymbol{R}))$ along the classical nuclear trajectory on the initial diabatic potential surface. Under the short time approximation, we can put

$$\Delta E_{if}(t) = -\Delta G - \lambda \quad (12)$$

where $-\Delta G$ is the free energy gap between the initial and final states and λ is the standard reorganization energy of the vibration and phonon. Then, eq 8 can be rewritten as

$$k_{DA}(-\Delta G) = \frac{1}{\hbar^2}\left\langle \int_{-\infty}^{\infty} dt\, T_{DA}^{q-c}(t) T_{AD}^{q-c}(0) D(t) \exp\left[\frac{i}{\hbar}(-\Delta G - \lambda)t\right]\right\rangle_T \quad (13)$$

where $k_{DA}(-\Delta G)$ indicates the ET rate from D to A with the energy gap $-\Delta G$. Here, we invoke a decorrelation assumption as done by Prezhdo and Rossky.[32] We factorize eq 13 as

$$k_{DA}(-\Delta G) = \frac{1}{\hbar^2}\int_{-\infty}^{\infty} dt\, \langle T_{DA}^{q-c}(t) T_{AD}^{q-c}(0)\rangle_T \langle D(t)\rangle_T \exp\left[\frac{i}{\hbar}(-\Delta G - \lambda)t\right] \quad (14)$$

In the classical approximation of vibrations and phonons, (FC) is written as

$$(FC) = \frac{1}{\sqrt{4\pi\lambda k_B T}} \exp\left[-\frac{(-\Delta G - \lambda)^2}{4\lambda k_B T}\right] \quad (15)$$

Performing the Fourier transform of (FC) in eq 15, we can write $\langle D(t)\rangle_T$ as

$$\langle D(t)\rangle_T = \exp[-\lambda k_B T t^2/\hbar^2] \quad (16)$$

Generally, Fourier transform of the product of two kinds of functions can be expressed by the convolution form of the respective Fourier transforms; namely, substituting eq 16 into eq 14 and performing the Fourier transform, we obtain

$$k_{DA}(-\Delta G) = \frac{2\pi}{\hbar}\frac{1}{\sqrt{4\pi\lambda k_B T}}\int_{-\infty}^{\infty} d\epsilon\, P(\epsilon) \exp\left[-\frac{(-\Delta G - \lambda - \epsilon)^2}{4\lambda k_B T}\right] \quad (17)$$

where $P(\epsilon)$ is the power spectrum obtained by the Fourier transform of $\langle T_{DA}^{q-c}(t) T_{AD}^{q-c}(0)\rangle_T$ as follows

$$P(\epsilon) = \frac{1}{2\pi\hbar}\int_{-\infty}^{\infty} dt\, \langle T_{DA}^{q-c}(t) T_{AD}^{q-c}(0)\rangle_T \exp[i\epsilon t/\hbar] \quad (18)$$

So far, we have followed the semiclassical treatment of $\langle T_{DA}^{q-c}(t) T_{AD}^{q-c}(0)\rangle_T$ by Prezhdo and Rossky.[32] However, if we assume that $\langle T_{DA}^{q-c}(t) T_{AD}^{q-c}(0)\rangle_T$ has a time-reversal symmetry, the following detailed-balance condition is not satisfied

$$k_{DA}(-\Delta G)/k_{AD}(\Delta G) = \exp[-\Delta G/k_B T] \quad (19)$$

where $k_{AD}(\Delta G)$ is the ET rate for the backward reaction A → D. This drawback happens when we use the classical MD simulation data having the time-reversal symmetry. Then, the quantum mechanical property for the movement of the frozen Gaussian wave packet must be recovered in the calculation of $\langle T_{DA}^{q-c}(t) T_{AD}^{q-c}(0)\rangle_T$. Oxtoby presented a prescription in order to escape from this drawback of the classical approximation as follows[36]

$$\int_{-\infty}^{\infty} dt\, \langle V_{ij}(t) V_{ji}(0)\rangle \exp(i\epsilon t/\hbar) \rightarrow \frac{2}{1+\exp(-\epsilon/k_B T)}\int_{-\infty}^{\infty} dt \left\langle \frac{1}{2}[V_{ij}(t), V_{ji}(0)]_+ \right\rangle \exp(i\epsilon t/\hbar) \quad (20)$$

where

$$[A,B]_+ = AB + BA \quad (21)$$

The term $[A,B]_+$ is symmetrical with time. Following this prescription, we rewrite $P(\epsilon)$ in eq 18 as follows

$$P(\epsilon) = \frac{2}{1+\exp(-\epsilon/k_B T)}\frac{1}{2\pi\hbar}\int_{-\infty}^{\infty} dt\, \langle T_{DA}(t) T_{AD}(0)\rangle_T \exp[i\epsilon t/\hbar] \quad (22)$$

where we dropped the superscript q−c from T_{DA} in order to discriminate from the previous T_{DA}^{q-c}. Since $T_{DA}(t)$ becomes the classical quantity in this stage, $T_{DA}(t)$ has the following property

$$T_{DA}(t) = T_{DA}(-t) \quad (23)$$

$$T_{AD}(0) = T_{DA}(0) \quad (24)$$

Then, we replace $\langle T_{DA}(t) T_{AD}(0)\rangle_T$ with $\langle T_{DA}(t) T_{DA}(0)\rangle_T$ hereafter. We can evaluate $\langle T_{DA}(t) T_{DA}(0)\rangle_T$ by the MD simulations and quantum chemical calculations of T_{DA}.

In the above, we treated the vibrations and phonons classically in the calculation of (FC) shown in eq 15. If we want to treat some groups of vibrations quantum mechanically, it is straightforward to extend the formula of eq 17 as[10,37]

$$k_{DA} = \frac{2\pi}{\hbar}\frac{1}{\sqrt{4\pi\lambda_1 k_B T}}\int_{-\infty}^{\infty} d\epsilon_1 \int_{-\infty}^{\infty} d\epsilon_2\, P(\epsilon_1) Q(\epsilon_2) \times \exp\left[-\frac{(-\Delta G - \lambda_1 - \epsilon_1 - \epsilon_2)^2}{4\lambda_1 k_B T}\right] \quad (25)$$

where $Q(\epsilon_2)$ is the Franck−Condon factor of the quantum vibrational modes and λ_1 is the reorganization energy of the residual vibrations and phonon.

The eq 17 or eq 25 with $P(\epsilon)$ of eq 22 is our final formula of the ET rate including the non-Condon effect. In the following we use eq 17 exclusively for simplicity.

To analyze the non-Condon effects on the ET rate, we divide eq 17 into two terms of elastic and inelastic tunneling mechanisms. For this purpose, we define the normalized autocorrelation function as follows

$$A(t) = \frac{\langle T_{DA}(t)T_{DA}(0)\rangle_T - \langle T_{DA}\rangle_T^2}{\langle T_{DA}^2\rangle_T - \langle T_{DA}\rangle_T^2} \tag{26}$$

where $\langle T_{DA}\rangle_T^2 \equiv \langle T_{DA}(0)\rangle_T^2$ and $\langle T_{DA}^2\rangle_T \equiv \langle T_{DA}^2(0)\rangle_T$. Here, $A(t)$ has the following property

$$-1 < A(t) \le 1 \quad \text{for} \quad t > 0 \tag{27}$$

$$A(t) = A(-t) \tag{28}$$

where the equality in eq 27 holds when no fluctuation of T_{DA} occurs. From eq 26, we obtain

$$\langle T_{DA}(t)T_{DA}(0)\rangle_T = (A(t) - 1)\{\langle T_{DA}^2\rangle_T - \langle T_{DA}\rangle_T^2\} + \langle T_{DA}^2\rangle_T \tag{29}$$

We adopt a mathematical principle that the power spectrum due to the inelastic mechanism should be zero when $A(t) = 1$ holds for all the time. Substituting eq 29 into eq 22, we express $P(\epsilon)$ by the sum of two terms

$$P(\epsilon) = P_{el}(\epsilon) + P_{inel}(\epsilon) \tag{30}$$

where

$$P_{el}(\epsilon) = \langle T_{DA}^2\rangle_T \delta(\epsilon) \tag{31}$$

$$P_{inel}(\epsilon) = \frac{2}{1 + \exp(-\epsilon/k_BT)} \frac{\langle T_{DA}^2\rangle_T - \langle T_{DA}\rangle_T^2}{2\pi\hbar} \times \int_{-\infty}^{\infty} dt\, (A(t) - 1) \exp[i\epsilon t/\hbar] \tag{32}$$

where $P_{el}(\epsilon)$ involves a factor $\delta(\epsilon)$ and is called the power spectrum due to the elastic tunneling mechanism, while $P_{inel}(\epsilon)$ involves a factor $(A(t) - 1)$ and is called the power spectrum due to the inelastic tunneling mechanism. Substituting eq 30 into eq 17, we obtain

$$k_{DA}(-\Delta G) = k_{DA}^{el}(-\Delta G) + k_{DA}^{inel}(-\Delta G) \tag{33}$$

where

$$k_{DA}^{el}(-\Delta G) = \frac{2\pi}{\hbar} \frac{1}{\sqrt{4\pi\lambda k_BT}} \int_{-\infty}^{\infty} d\epsilon\, P_{el}(\epsilon) \times \exp\left[-\frac{(-\Delta G - \lambda - \epsilon)^2}{4\lambda k_BT}\right] = \frac{2\pi}{\hbar} \frac{\langle T_{DA}^2\rangle_T}{\sqrt{4\pi\lambda k_BT}} \times \exp\left[-\frac{(-\Delta G - \lambda)^2}{4\lambda k_BT}\right] \tag{34}$$

$$k_{DA}^{inel}(-\Delta G) = \frac{2\pi}{\hbar} \frac{1}{\sqrt{4\pi\lambda k_BT}} \int_{-\infty}^{\infty} d\epsilon\, P_{inel}(\epsilon) \times \exp\left[-\frac{(-\Delta G - \lambda + \epsilon)^2}{4\lambda k_BT}\right] = \frac{1}{\hbar^2} \frac{\langle T_{DA}^2\rangle_T - \langle T_{DA}\rangle_T^2}{\sqrt{4\pi\lambda k_BT}} \int_{-\infty}^{\infty} d\epsilon \int_{-\infty}^{\infty} dt\, (A(t) - 1) \times \exp(i\epsilon t/\hbar) \frac{2}{1 + \exp(-\epsilon/k_BT)} \exp\left[-\frac{(-\Delta G - \lambda + \epsilon)^2}{4\lambda k_BT}\right] \tag{35}$$

The expression of k_{DA}^{el} of eq 34 just corresponds to k_{DA} in the slow modulation limit of eq 2.

It should be emphasized here that the elastic tunneling mechanism is defined without ambiguity by its power spectrum involving only the delta function of energy. It should be also emphasized that the inelastic tunneling mechanism is reasonably defined so that k_{DA}^{inel} may become zero when the thermal fluctuation of T_{DA} does not happen and $A(t) = 1$ holds. In the case of slow modulation of T_{DA}, the factor $(A(t) - 1)$ becomes much smaller than 1 for long time range and causes k_{DA}^{inel} much less than k_{DA}^{el}. This is the reason k_{DA}^{el} is called the ET rate in the slow modulation limit.

The fact that the detailed balance condition (eq 19) is satisfied for k_{DA} in eq 33 is proved in Appendix A.

3. Method

3.1. Molecular Dynamics. Molecular dynamics (MD) simulations were performed by the same procedures as described in the first paper of this series of study.[18] The initial configuration of the reaction center of *Rhodobacter sphaeroides* was obtained from the Protein Data Bank, entry code 1AIJ.[38] The 262 water molecules incorporated in the structure 1AIJ are taken into account after optimization of their positions. The number of atoms used for MD is 14 631. The MD program PRESTO[39] was used with the AMBER force field.[40] We adopted a dielectric constant of 2 and approximated Coulomibic potentials over 12 Å by the PPPC method.[41] The harmonic restriction was imposed on the heavy atoms in the surface residues of the protein. The same restriction was imposed on oxygen atoms of water molecules. The SHAKE algorithm[42] was used for bond stretchings of hydrogen atoms. The system was kept at 300 K. An integration time step of 1 fs was employed. After 160 ps of equilibration, we generated a trajectory for 515 ps. We collected the conformation at every 1 fs, which was used to calculated T_{DA}.

3.2. Electronic Structure Calculations. In the calculation of T_{DA} for each protein conformation, we adopt a pruned system which consists of Bph, Q_A, and the three amino acids Trp^{M252}, Met^{M218}, and His^{M219}. The molecular configuration is shown in Figure 1. The long hydrocarbon chains of native bacteriopheophytin *a* and the native ubiquinone 10 are truncated to hydrogen atoms. In our previous works,[18] we showed that these three amino acids are necessary and sufficient to calculate T_{DA} in the electron transfer from Bph^- to Q_A.

The electronic states of the pruned protein were solved at the extended Hückel level. We referred to the FORTICON8 program[43] for the extended Hückel calculations. We used a ITPACK 2C[44] package for solving the secular equations. To calculate electronic structures of donor and acceptor, the PM3 method[45] in the GAUSSIAN package[46] was used.

Since we are considering the electron transfer from Bph^- to Q_A, the lowest unoccupied molecular orbital of the neutral Bph

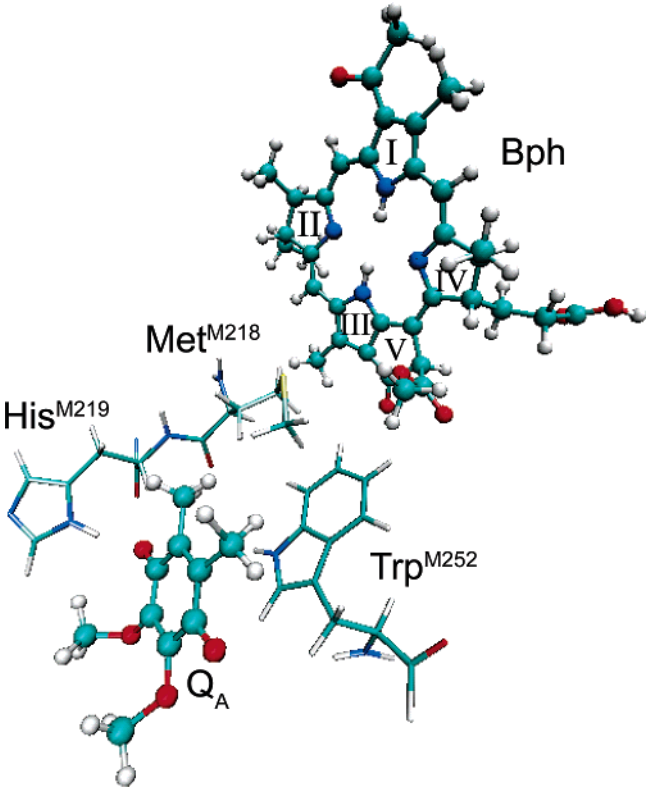

Figure 1. Molecular configurations of Bph (donor), Q_A (acceptor), and important three amino acids Trp^{M252}, Met^{M218}, and His^{M219} in the ET of the reaction center of *Rhodobacter sphaeroides*.

is chosen as the molecular orbital of donor ϕ_D and the lowest unoccupied molecular orbital of the neutral Q_A is chosen as the molecular orbital of acceptor ϕ_A. The calculation of T_{DA} for each protein conformation was made by the same method as the previous one.[15,18,47−49] However, in the present study, we need to calculate T_{DA} values of many conformations of protein. To save the computational time, we fix the atomic orbital coefficients in ϕ_D and ϕ_A which are solved in the isolated state of Bph and Q_A, respectively. A possible effect of this approximation is discussed in the latter section.

4. Results

4.1. Dynamics of the Tunneling Matrix Element T_{DA}. Figure 2 shows an example of the time-dependent T_{DA} calculated at every 1 fs for 15 ps for the electron transfer from Bph^- to Q_A. The red line is the result calculated by using the 3 amino acids as a protein environment. The green line is the result calculated by using the 13 amino acids which nearly surround the donor and acceptor as a protein environment. We see that very rapid fluctuation of T_{DA} takes place. From this figure, we confirm that the fluctuation of T_{DA} of the green line coincides very well with the red line. The inset shows the expanded graph for 0−500 fs. We see some kind of oscillation with period of 20−30 fs time scale. This kind of oscillation was observed before in the calculation of T_{DA} of another protein system, Ru-modified azurin.[11]

On the basis of the calculated time course of $T_{DA}(t)$ for 515 ps, we calculated the normalized autocorrelation function $A(t)$ defined in eq 26 for the correlation function $\langle T_{DA}(t)T_{DA}(0)\rangle_T$. Figure 3 shows the time dependence of the normalized autocorrelation function $A(t)$. The red curve of $A(t)$ using the simulation data of T_{DA}. We see that this $A(t)$ decays smoothly and rather rapidly: $A(t)$ becomes 0.5 at about 65 fs. This decay

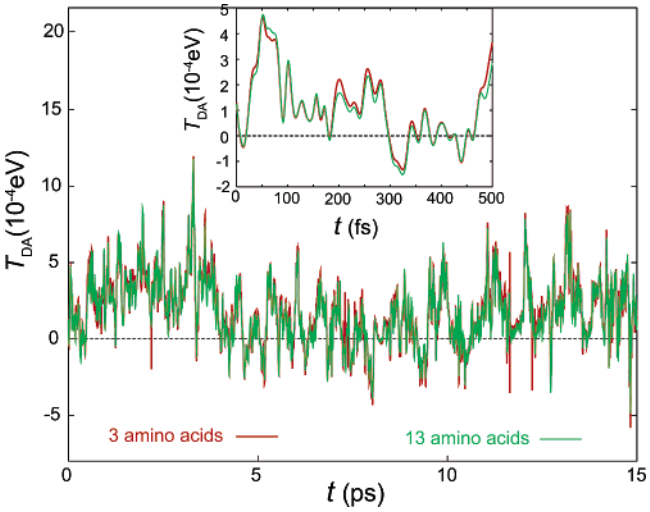

Figure 2. Time dependence of T_{DA} calculated at every 1 fs. Red lines correspond to the case where 3 amino acids are used as a protein mediator. Green lines correspond to the case where 13 amino acids are used as a protein mediator.

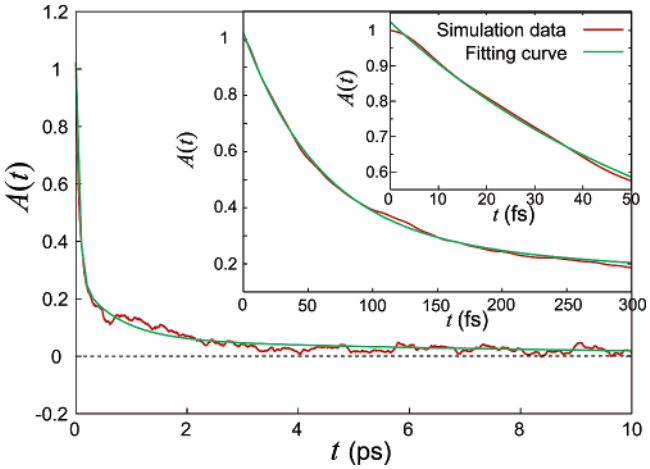

Figure 3. Time dependence of the normalized autocorrelation function $A(t)$. The red line represents $A(t)$ calculated using the simulation data of $T_{DA}(t)$. The green line represents $A(t)$ obtained by the best fit to the red line with use of an empirical function made of three exponentials.

time is similar to that of Ru-modified azurin.[19] We performed the global curve fitting of $A(t)$ between 0 and 10 ps by using three exponential forms. The fitted curve by the nonlinear least-squares method is as follows

$$A(t) = 0.751\exp[-t/60.3] + 0.211\exp[-t/720] + 0.062\exp[-t/8490] \quad (36)$$

This theoretical curve is shown as the green line in Figure 3. Comparing the red curve with the green curve, we find that the coincidence between the two curves is generally good over the whole time region from 0 to 10 ps. However, we observe that a small amount of oscillation in the red curve exists with a period of about 20−30 fs in the early time region until about 90 fs. We also observe that the red curve is downward concaved in the time region from 0 to about 8 fs.

Figure 4 shows the power spectrum $P(\epsilon)$ calculated using eq 22. This $P(\epsilon)$ has an asymmetrical shape about $\epsilon = 0$ due to the prefactor of the integral (quantum correction factor) in eq 22. We see that the calculated $P(\epsilon)$ has a sharp peak at 0 cm^{-1}. The calculated $P(\epsilon)$ has notable broad peaks at 1400−2000 cm^{-1} owing to the oscillations of $A(t)$ before 90 fs as seen in the

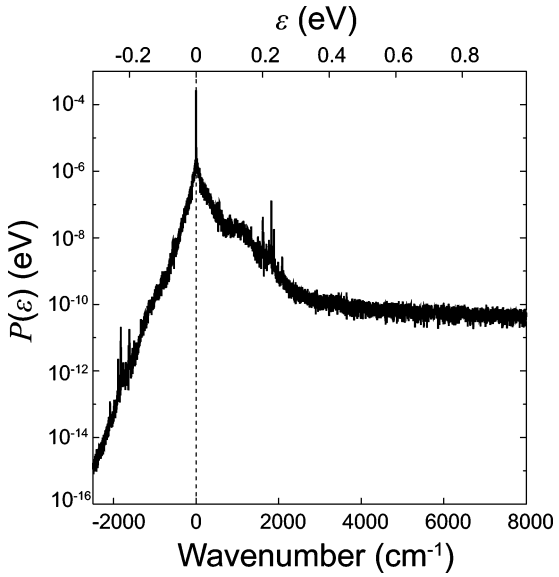

Figure 4. The calculated power spectrum $P(\epsilon)$ using the simulation data of the time correlation function of $T_{DA}(t)$ and eq 22.

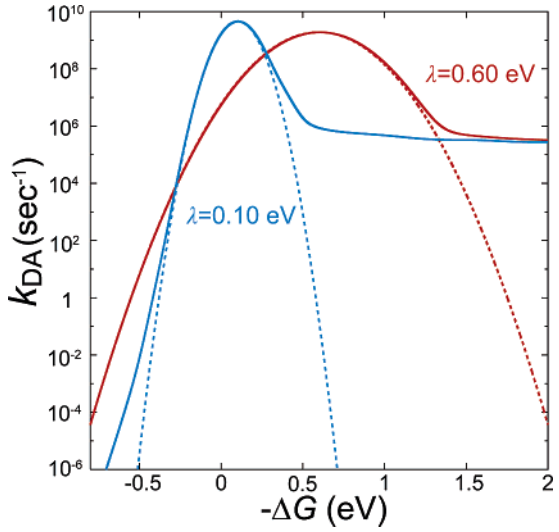

Figure 5. The energy gap dependence of the ET rate k_{DA} for $\lambda = 0.60$ eV (red line) or $\lambda = 0.10$ eV (blue line). The solid lines represent k_{DA} calculated by the present non-Condon theory. The broken lines represent k_{DA}^{el} having a shape of Marcus' parabola.

insets of Figure 3. We observe that the global form of $P(\epsilon)$ is a Lorentzian type at the large value of ϵ and keeps a considerable amplitude at the wavenumber larger than 3000 cm^{-1}.

4.2. Energy Gap Laws of the ET Rate k_{DA}. We calculate the electron-transfer rate k_{DA} by using eq 17. In this, we choose 0.60 eV for the reorganization energy λ referring to the experimental data of the energy gap law for the ET from Bph^{-1} to Q_A.[2,50] In Figure 5, we show the logarithm of the calculated ET rate k_{DA} as a function of the energy gap $-\Delta G$ by the solid red line. For comparison, we plot k_{DA}^{el} by the broken red line which is equivalent to k_{DA} of the slow modulation limit in eq 2. The broken red curve is the so-called Marcus' parabola with a maximum at $-\Delta G = 0.60$ eV. The solid red curve has a maximum value 1.89×10^9 s^{-1} at the energy gap 0.605 eV. This maximum value of k_{DA} agrees rather well with the experimental value 1×10^9 s^{-1}.[2,50] It appears that the coincidence of the broken red curve and the solid red curve is very good in the normal region ($-\Delta G < \lambda$) and is also good until about 1.0 eV in the inverted region ($-\Delta G > \lambda$). A large deviation happens between the two curves at the larger energy gap in the inverted region. Namely, k_{DA} decreases very slowly for $-\Delta G > 1.3$ eV. The value of k_{DA} in this nearly constant region is smaller than the maximum value by about 4 orders of magnitude. Since the deviation of the inverted region of k_{DA} from the Marcus' parabola is very large, we call it the anomalous inverted region. The similar anomaly of the energy gap law also happens at the large uphill energy gap in the normal region, although it is not seen in the plotted energy gap range. To see it, we draw the curve of k_{DA} calculated using the smaller value of the reorganization energy 0.10 eV. The solid blue curve corresponds to k_{DA} of eq 17 and the broken blue curve corresponds to k_{DA}^{el}. In this case, the maximum of the energy gap law locates at $-\Delta G = 0.10$ eV. The solid blue curve remarkably deviates from the broken blue curve for the energy gap larger than 0.25 eV and apparently approaches a constant value for $-\Delta G > 0.6$ eV. The value of this nearly constant value almost coincides with that of the solid red curve. The solid blue curve also deviates largely from the broken blue curve for $-\Delta G < -0.40$ eV in the normal region. Namely, the decrease of the solid blue curve becomes dull as the energy gap $-\Delta G$ becomes negatively large. A very slow decrease of k_{DA} at the larger energy gap in the inverted region is concomitant with a dull decrease of k_{DA} at the smaller energy gap in the normal region. Namely, these two anomalies appear in a pair because $k_{DA}(-\Delta G)$ and $k_{AD}(\Delta G)$ satisfy the condition of the detailed balance in eq 19. Hereafter, we call the energy gap region of the large deviation of k_{DA} from the Gaussian curve as the anomalous region for convenience.

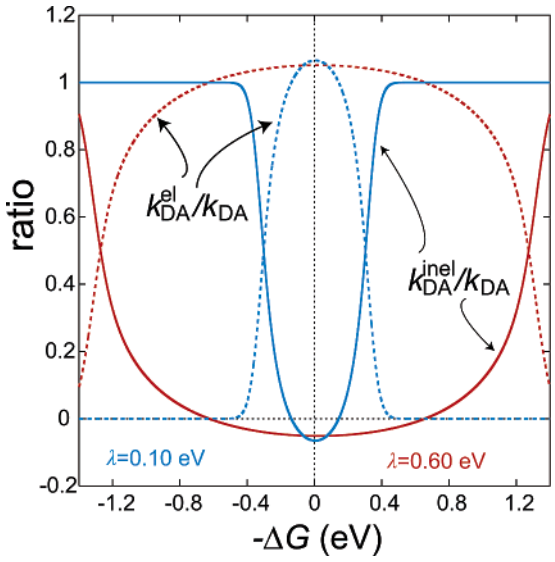

Figure 6. Calculated ratios k_{DA}^{el}/k_{DA} (broken line) k_{DA}^{inel}/k_{DA} (solid line) as a function of the energy gap. The red line corresponds to $\lambda = 0.60$ eV, and the blue line corresponds to $\lambda = 0.10$ eV.

4.3. Effects of the Inelastic Tunneling on the ET Rate. We investigated the effects of the inelastic tunneling on the ET rate. For this purpose, we divide k_{DA} into k_{DA}^{el} and k_{DA}^{inel} using eqs 34 and 35. It should be noted that k_{DA}^{el} is equivalent to k_{DA} in the slow modulation limit given in eq 2. In Figure 6, we plot the calculated ratios of k_{DA}^{el}/k_{DA} and k_{DA}^{inel}/k_{DA} for $\lambda = 0.60$ eV as a function of $-\Delta G$ by the broken red line and the solid red line, respectively. The solid red line (k_{DA}^{inel}/k_{DA}) is negative in the region -0.64 eV $< -\Delta G < 0.64$ eV with a minimum at $-\Delta G = 0$ eV. The solid red line is positive in the region $|-\Delta G| > 0.64$ eV and increases rapidly with increase of $|-\Delta G|$ in the region $|-\Delta G| > 0.64$ eV. The ratio becomes 0.9 at $|-\Delta G| = 1.3$ eV. The broken red line ($k_{DA}^{el}/k_{DA}^{inel}$) shows the behavior of the mirror image of the solid red line with respect to the line of

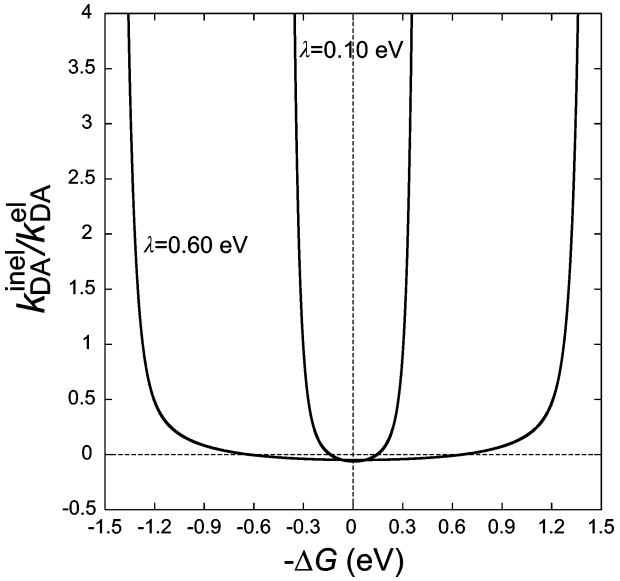

Figure 7. Calculated ratio $k_{DA}^{inel}/k_{DA}^{el}$ as a function of the energy gap for $\lambda = 0.60$ or 0.10 eV.

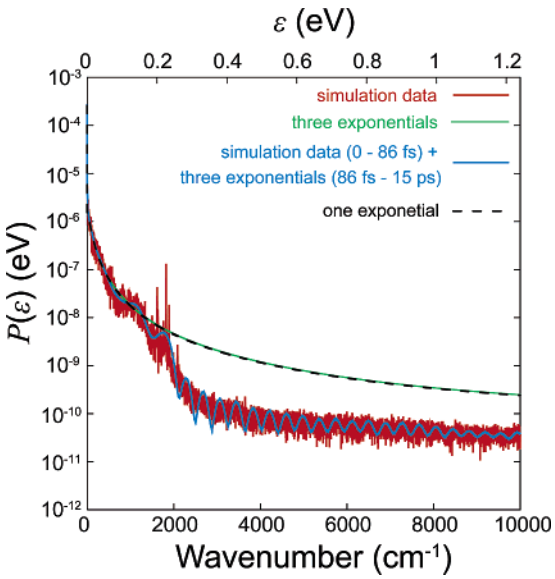

Figure 8. Comparison of the power spectra $P(\epsilon)$ obtained by the various methods. The red line is obtained by using the simulation data (same as Figure 4). The green line is obtained by using three kinds of exponentials of eq 36. The blue line is obtained by using a composite $A(t)$; the simulation data of $A(t)$ in the time region 0−86 fs and the three kinds of exponentials in the time larger than 86 fs. The broken black line is obtained by using the first exponential term of eq 36.

the ratio 0.5. At the matching condition $-\Delta G = 0.60$ eV in the Marcus theory, k_{DA}^{inel}/k_{DA} is almost zero, which is even smaller than the previous calculations[23,27]

To see the rapidly increasing property of the solid red line more exactly, we plot the calculated ratios of k_{DA}^{el}/k_{DA} and k_{DA}^{inel}/k_{DA} for $\lambda = 0.10$ eV as a function of $-\Delta G$ by the broken blue line and the solid blue line, respectively. The solid blue line (k_{DA}^{inel}/k_{DA}) is negative in the region -0.14 eV $< -\Delta G <$ 0.14 eV with a minimum at $-\Delta G = 0$ eV. The solid blue line is positive in the region $|-\Delta G| > 0.14$ eV and increases very rapidly with increase of $|-\Delta G|$ in the region $|-\Delta G| > 0.14$ eV. The solid blue line becomes 0.96 at $|-\Delta G| = 0.40$ eV. In the region $|-\Delta G| > 0.40$ eV, the solid blue line approaches 1.00 very quickly for $|-\Delta G| > 0.40$ eV. The broken blue line (k_{DA}^{el}/k_{DA}) shows the behavior of the mirror image of the solid blue line with respect to the line of the ratio 0.5.

Summarizing the above results, we may conclude that the ratios of k_{DA}^{el}/k_{DA} and k_{DA}^{inel}/k_{DA} as a function of the energy gap are symmetrical with respect to $-\Delta G = 0$ for both cases of λ. The inelastic tunneling mechanism contributes to decelerate the ET rate in the energy gap range $-a\lambda < -\Delta G < a\lambda$ where a is a constant close to 1 weakly dependent on λ: $a = 1.07$ for $\lambda = 0.60$ eV and $a = 1.40$ for $\lambda = 0.10$ eV. The inelastic tunneling mechanism contributes to accelerate the ET rate in the energy gap range $|-\Delta G| > a\lambda$.

Next, we investigate the relative contribution of the inelastic and elastic mechanisms to k_{DA}. This kind of study was made before by the second-order perturbation method by Troisi et al.[27] Namely, they derived an equation where $k_{DA}^{inel}/k_{DA}^{el}$ as a function of the energy gap is expressed as a parabola with a minimum at $-\Delta G = \lambda$. Therefore, it is interesting to compare our result with theirs. In Figure 7, we plot our calculated value of $k_{DA}^{inel}/k_{DA}^{el}$ as a function of the energy gap for $\lambda = 0.6$ and 0.10 eV, respectively. We find that our curves are nearly parabola in the range $|-\Delta G| < 1.5\lambda$ with a minimum at $-\Delta G = 0$. The difference of the minimum position is due to whether the detailed balance condition is satisfied or not. Although the position of the minimum is different between the two results, the parabolic property is similar. However, we find that the curve in Figure 7 increases drastically for $|-\Delta G| > 2\lambda$. In this region of the energy gap, the inelastic tunneling mechanism prevails and the second-order perturbation method is not applicable.

5. Discussion

5.1. Origin of the Long Tail in $P(\epsilon)$. In Figure 4, we obtained the power spectrum $P(\epsilon)$ with a very long tail which decays very slowly until 8000 cm^{-1}. One may point out that this long tail might be due to noise effects. Indeed, the above power spectrum was calculated by using a finite size of ensemble of $T_{DA}(t)$ obtained by the MD simulation. Therefore, there might be a possibility that an incomplete sampling may cause some noise effect to $P(\epsilon)$. In this subsection, we examine whether the long tail in $P(\epsilon)$ is an intrinsic property or indicative of a noise effect due to a finite number of sampling in the simulation data.

In Figure 3, we showed that the time course of the simulation data of $A(t)$ (red curve) is well fitted by an empirical curve made of three kinds of exponential functions represented by the green curve. The formula of the empirical curve is written in eq 36. The dominant term (with amplitude 0.751) decays with a time constant τ_c, which we call the correlation time, of 60.3 fs. The second dominant term (with amplitude 0.211) decays with $\tau_c = 720$ fs. The most minor term (with amplitude 0.062) decays with $\tau_c = 8490$ fs. The last term contributes significantly to $A(t)$ only at the time larger than 1.5 ps in Figure 3.

Using the empirical curve, we calculated the power spectrum $P(\epsilon)$ of eq 22. The result is plotted by the green curve in Figure 8 together with the simulation data (red line). We plotted $P(\epsilon)$ only in the positive region of ϵ for convenience. We find that the green curve fits the red line very well until the wavenumber 1300 cm^{-1} and deviates upward from the red line after 1300 cm^{-1}. The deviation becomes maximum (by about a one and a half order of magnitude) at 3000 cm^{-1} and gradually becomes smaller (by about 1 order of magnitude at 10 000 cm^{-1}). The green curve fails to reproduce the bumps at around 1300 and 1700 cm^{-1} in the red curve. To clarify the reason of the above discrepancy, we produce an artificially connected $A(t)$ as follows.

In the time region 0−86 fs, we use $A(t)$ of the simulation data. In the time region larger than 86 fs, we use $A(t)$ of the empirical curve made of the three exponentials (eq 36). When we use this connected $A(t)$, we obtain $P(\epsilon)$ as shown by the blue curve in Figure 8. Interestingly, the blue curve globally follows the red curve in the whole range of ϵ. To see the detail, the two bumps at around 1300 and 1700 cm^{-1} of the red curve are reproduced by the blue curve. The lower level of the long tail of the red curve over the green curve in the region of wavenumber larger than 2000 cm^{-1} is also qualitatively reproduced by the blue curve although the blue curve oscillates within the broad width of the red curve. From this result, we can conclude as follows. The replacement of the empirical curve of $A(t)$ in the time region 0−86 fs with the simulation curve which involves the effect of oscillations of $T_{DA}(t)$ with period of 20−30 fs as seen in the *inset* of Figure 2 not only produces two bumps at around 1300 and 1700 cm^{-1} but also contributes to lower the level of the long tail of the green curve by a one and a half order of magnitude at around 2500 cm^{-1} and by a 1 order of magnitude at around 10 000 cm^{-1}. The two bumps can be ascribed to the contribution of two kinds of high-frequency vibrations. The peak separation in the oscillation of the blue curve in the region of wavenumbers larger than 2000 cm^{-1} of Figure 8 is about 390 cm^{-1} which corresponds to a period of about 86 fs. Therefore, we find that the above oscillation of the blue curve was produced by the effect of connecting the nonsmooth red curve of $A(t)$ with the smooth green curve of $A(t)$ at 86 fs in Figure 3. Similarly, we can ascribe the origin of the broad width of the red curve in $P(\epsilon)$ to the random fluctuation of the red curve of $A(t)$ around the smooth green curve of $A(t)$ in the time region larger than 86 fs in Figure 3.

To specify the form of $A(t)$ in the early time region in more detail, we calculate $P(\epsilon)$ using only the dominant exponential term in eq 36. The result is plotted by the broken black curve in Figure 8. We find that the broken black curve almost completely fits the green curve for all the ϵ values except for the region of the very small value of ϵ. This fact indicates that the dominant exponential term (with the shortest correlation time) in $A(t)$ determines the basic form of the long tail of $P(\epsilon)$. To put this more concretely, the long tail of the green curve in Figure 8 is essentially expressed by a Lorentzian form which is a Fourier transform of the exponential function, although it is a little modified by the quantum correction term in eq 22. The actual form of $P(\epsilon)$ is formed by adding the high-frequency vibrational effect stated above to this Lorentzian form.

Judging from all the above results, we conclude that the origin of the long tail of $P(\epsilon)$ in Figure 8 is not due to a noise effect which might occur due to a finite number of conformations in the ensemble but is an intrinsic property which is brought about by a specific form of $A(t)$ in the early time region (less than 86 fs).

It is evident that the long tail in $P(\epsilon)$ produces the anomalous inverted region in which k_{DA} is much enhanced from the Marcus' parabola at the larger energy gap in the inverted region.

5.2. Origin of the Symmetrical Property of k_{DA}^{inel}/k_{DA} and k_{DA}^{el}/k_{DA} with respect to $-\Delta G = 0$. In Figures 6 and 7, we showed numerically that the ratios k_{DA}^{inel}/k_{DA}, k_{DA}^{el}/k_{DA}, and $k_{DA}^{inel}/k_{DA}^{el}$ as a function of the energy gap are symmetrical with respect to $-\Delta G = 0$. It should be remembered here that $k_{DA} = k_{DA}^{el} + k_{DA}^{inel}$ holds and that k_{DA}^{el} is equivalent to k_{DA} in the slow modulation limit. In the following, we theoretically prove that the above symmetrical property of the ratios always holds true.

As we proved in the Appendix, $k_{DA}^{inel}(-\Delta G)$, $k_{DA}^{el}(-\Delta G)$, and $k_{DA}(-\Delta G)$ satisfy the following detailed balance condition

$$k_{DA}^{inel}(-\Delta G) = k_{AD}^{inel}(\Delta G)\exp(-\Delta G/k_B T) \tag{37}$$

$$k_{DA}^{el}(-\Delta G) = k_{AD}^{el}(\Delta G)\exp(-\Delta G/k_B T) \tag{38}$$

$$k_{DA}(-\Delta G) = k_{AD}(\Delta G)\exp(-\Delta G/k_B T) \tag{39}$$

where $-\Delta G$ indicates the free energy difference for the forward (D → A) reaction and ΔG indicates the free energy difference for the backward (A → D) reaction.

Then, these ratios satisfy the following relations:

$$\frac{k_{DA}^{inel}(-\Delta G)}{k_{DA}(-\Delta G)} = \frac{k_{AD}^{inel}(\Delta G)}{k_{AD}(\Delta G)} \tag{40}$$

$$\frac{k_{DA}^{el}(-\Delta G)}{k_{DA}(-\Delta G)} = \frac{k_{AD}^{el}(\Delta G)}{k_{AD}(\Delta G)} \tag{41}$$

$$\frac{k_{DA}^{inel}(-\Delta G)}{k_{DA}^{el}(-\Delta G)} = \frac{k_{AD}^{inel}(\Delta G)}{k_{AD}^{el}(\Delta G)} \tag{42}$$

Equations 40−42 indicate that k_{DA}^{inel}/k_{DA}, k_{DA}^{el}/k_{DA}, and $k_{DA}^{inel}/k_{DA}^{el}$ as a function of the energy gap are symmetrical with respect to $-\Delta G = 0$. These results give a physical reasoning why the ratios in Figures 6 and 7 are symmetrical with respect to $-\Delta G = 0$.

Here we compare the present results with the previous works treating non-Condon effects on the energy gap law. In most of the previous works, a symmetrical correlation function $\langle T_{DA}(t)T_{DA}(0)\rangle = \langle T_{DA}(-t)T_{DA}(0)\rangle$ was assumed. Then, a result where the non-Condon effect appears by keeping the symmetry of the energy gap law with respect to $-\Delta G = \lambda$ was obtained.[23,24,27,28] These calculated ET rates do not satisfy the detailed balance condition. It is essential to satisfy the detailed balance condition in order to correctly evaluate the non-Condon effect in the energy gap law. In the study by Deizadeh et al., the detailed balance condition would be approximately satisfied because they used only a high-frequency vibrational mode with large wavenumber for the non-Condon effect.[11,25] However, as we have shown in Figure 8, the role of the high-frequency vibrational mode is small and the essential part of the non-Condon effect is obtained by the exponential decay of the autocorrelation function at least in our system.

5.3. Population Analysis of T_{DA} and T_{DA}^2. Using Figure 6, we concluded that the ratio k_{DA}^{el}/k_{DA} becomes 1 at $-\Delta G = a\lambda$ where a is close to 1. The condition $-\Delta G = \lambda$ indicates that the matching condition is satisfied in the Marcus parabola and the ET rate becomes maximum. Combining the above two facts, we can say that k_{DA} is nearly equal to k_{DA}^{el} at the energy gap giving the maximum ET rate

$$k_{DA}(-\Delta G) \sim \frac{2\pi}{\hbar}\frac{\langle T_{DA}{}^2\rangle}{\sqrt{4\pi\lambda k_B T}} \tag{43}$$

In such an expression, the correct evaluation of the electronic factor $\langle T_{DA}{}^2\rangle$ becomes important. In the following, we investigate which part of fluctuating T_{DA} contributes significantly to $\langle T_{DA}{}^2\rangle$ using the simulation data.

We use the data of T_{DA} calculated for 500 000 configurations sampled at every 1 fs in the MD simulation. We name T_{DA}^{MAX} and T_{DA}^{MIN} for the maximum and minimum of T_{DA} in the simulation data, respectively. Then, we divide the total range $T_{DA}^{MAX} - T_{DA}^{MIN}$ into N sections. We label each section of T_{DA} by i ($i = 1, \cdots, N$) as follows

$$T_{\mathrm{DA}}^{i} = T_{\mathrm{DA}}^{\mathrm{MIN}} + \frac{i-\frac{1}{2}}{N}(T_{\mathrm{DA}}^{\mathrm{MAX}} - T_{\mathrm{DA}}^{\mathrm{MIN}}) \qquad (44)$$

Then, we count the population of $T_{\mathrm{DA}}(t)$ which belongs to ith section with the T_{DA} value from $(T_{\mathrm{DA}}^{\mathrm{MAX}} - T_{\mathrm{DA}}^{\mathrm{MIN}})(i-1)/N$ to $(T_{\mathrm{DA}}^{\mathrm{MAX}} - T_{\mathrm{DA}}^{\mathrm{MIN}})i/N$. This population is named f_i.

In Figure 9, we draw the graph of f_i as a function of T_{DA}^{i}, by adopting $N = 132$. In the same figure, we plotted a Gaussian function with a broken line which is obtained by the best fitting to the distribution of f_i. We find that the distribution of f_i is nearly symmetrical and it is close to the Gaussian function except for the existence of small skewness and a little higher tail than that of the Gaussian function. Therefore, we can say that the distribution of T_{DA}^{i} mostly follows the normal distribution in a stochastic theory.[51] We marked the positions of $T_{\mathrm{DA}}^{\mathrm{MAX}}$, $T_{\mathrm{DA}}^{\mathrm{MIN}}$, $\langle T_{\mathrm{DA}}\rangle$, and $\langle|T_{\mathrm{DA}}|\rangle$ by the arrows.

Using these data, we define the participation ratio B_i of $(T_{\mathrm{DA}}^{i})^2$ to $\langle T_{\mathrm{DA}}{}^2\rangle$ as follows

$$B_i \equiv \frac{f_i(T_{\mathrm{DA}}^{i})^2}{\langle T_{\mathrm{DA}}{}^2\rangle} \qquad (45)$$

In Figure 10, we plotted B_i as a function of $|T_{\mathrm{DA}}^{i}|$. The distribution of B_i looks like a Poisson distribution function having a large skewness. A long tail exists at the larger value of $|T_{\mathrm{DA}}^{i}|$. The large values of B_i locate at a region 4×10^{-4} to 5×10^{-4} eV of $|T_{\mathrm{DA}}^{i}|$. The B_i value at $|T_{\mathrm{DA}}^{\mathrm{N}}|$, which is a section including $T_{\mathrm{DA}}^{\mathrm{MAX}}$, is only 0.00012. As shown in the figure, $\langle T_{\mathrm{DA}}{}^2\rangle = 8.82 \times 10^{-8}$ (eV^2) while $(T_{\mathrm{DA}}^{\mathrm{MAX}})^2 = 2.71 \times 10^{-6}$ (eV^2). Therefore, $(T_{\mathrm{DA}}^{\mathrm{MAX}})^2$ overestimates the value of $\langle T_{\mathrm{DA}}{}^2\rangle$ by about 30 times. It is not in our case that the strongest coupled conformers dominate the electron-transfer rate.[20] The *inset* of Figure 2 shows that $T_{\mathrm{DA}}(t)$ has components of oscillation with a period of 20−30 fs riding on a large scale of fluctuations. This result indicates that T_{DA} values of many conformations must be collected for taking a reasonable ensemble average of $T_{\mathrm{DA}}{}^2$.

Figure 10 represents that $|T_{\mathrm{DA}}^{i}|$ values in the region 4×10^{-4} to 5×10^{-4} eV maximally contribute to B_i. On the other hand, $\langle T_{\mathrm{DA}}{}^2\rangle^{1/2}$ is 2.97×10^{-4} eV as shown by the white arrow, which is located at the much smaller value than the $|T_{\mathrm{DA}}^{i}|$ values corresponding to the maximum region of B_i. This fact indicates that we should not estimate the $\langle T_{\mathrm{DA}}{}^2\rangle$ value by the square of $|T_{\mathrm{DA}}^{i}|$ which gives the maximum of B_i. This difference is not easily understood intuitively. The mathematical reasoning for this difference is shown in Appendix B.

The data of Figures 9 and 10 indicate that the ratio $\langle T_{\mathrm{DA}}\rangle^2/\langle T_{\mathrm{DA}}{}^2\rangle = 0.405$ holds. This value is six times larger than 0.067 which was obtained in our previous study for the same system.[18] The reason for this difference is as follows: The coefficients of atomic orbitals in the molecular orbitals of donor ϕ_D and acceptor ϕ_A are fixed in the present study while they were not fixed in the previous study. We found that the methyl group linked to the ring III of Bph and the methyl group linked to the quinone ring rotate during the time course of MD simulation. Both methyl groups work as important elements of the Met route which contributes to make T_{DA} negative.[18] The coefficients of atomic orbitals among the three hydrogen atoms of methyl groups are different. When the molecular orbitals of ϕ_{D} and ϕ_{A} are fixed, the Met route can change between the nearly open state and nearly closed state by the rotation of methyl groups. Numerically, we find that the global center of the fluctuation

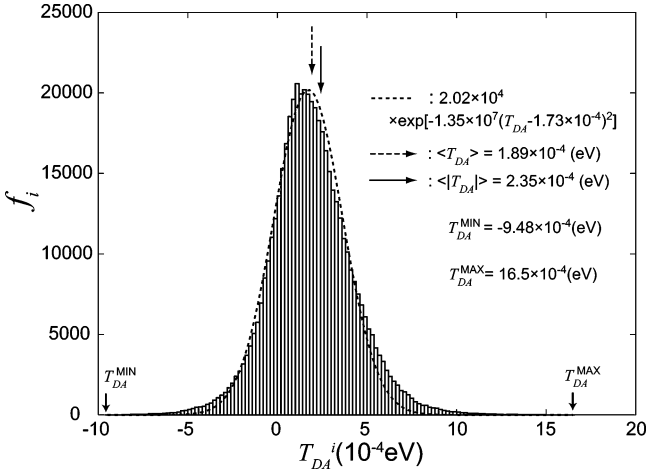

Figure 9. Plot of the number of occasions f_i of T_{DA}^{i} among 500 000 events. The broken line represents the best fitted Gaussian function.

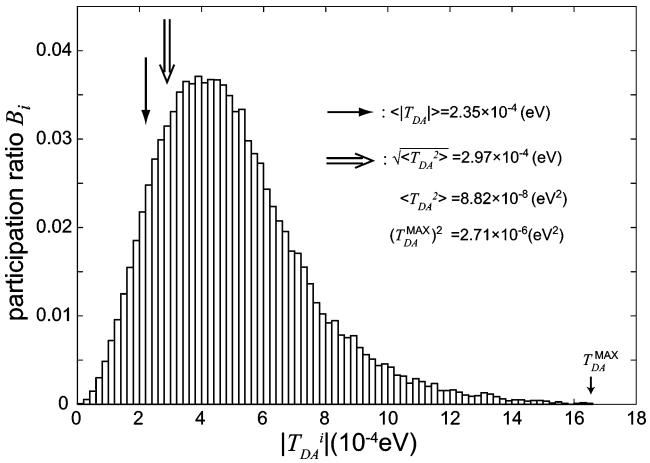

Figure 10. Plot of the participation ratio B_i as a function of $|T_{\mathrm{DA}}^{i}|$.

of $T_{\mathrm{DA}}(t)$ in Figure 2 in this paper is shifted to the positive side of T_{DA} as compared with that in Figure 7 of the previous paper, indicating that the Met route is less effectively used for $T_{\mathrm{DA}}(t)$, and the ratio $\langle T_{\mathrm{DA}}\rangle^2/\langle T_{\mathrm{DA}}{}^2\rangle$ becomes large in the present study. It should be emphasized, however, that this alteration of the fluctuation of $T_{\mathrm{DA}}(t)$ does not significantly affect the property of $A(t)$ or $P(\epsilon)$ because the rotation time scale of the methyl group is much larger than the fluctuation time scale of $T_{\mathrm{DA}}(t)$ which is effective for producing the notable non-Condon effect.

5.4. Dependence of the Anomalous Inverted Region on the Correlation Times of $A(t)$. In this subsection, we discuss how the anomalous inverted region depends on the form of $A(t)$. In Figure 8, we showed that $P(\epsilon)$ theoretically calculated by using a single exponential form of $A(t)$ fits well with $P(\epsilon)$ of the simulation until about 2000 cm^{-1} but that the theoretical curve (broken black curve) becomes about 1 order of magnitude higher than the simulation data (red curve) after 2000 cm^{-1}. We express a theoretical curve for $A(t)$ as

$$A(t) = \exp\left(-\frac{|t|}{\tau_{\mathrm{c}}}\right) \qquad (46)$$

where τ_{c} is the effective correlation time. We expect that $P(\epsilon)$ calculated using a single exponential form of $A(t)$ and by adjusting τ_{c} to a little small value would roughly fit the long tail of $P(\epsilon)$.

When we adopt $A(t)$ in eq 46, we can rewrite k_{DA} of eq 33 as

$$k_{DA}(-\Delta G) = WC \exp\left[-\frac{(-\Delta G - \lambda)^2}{4\lambda k_B T}\right] + W(1-C)\frac{1}{\pi}\int_{-\infty}^{\infty} d\epsilon \frac{2}{1+\exp(-\epsilon/k_B T)} \frac{\hbar\gamma}{\epsilon^2 + \hbar^2\gamma^2} \times \exp\left[-\frac{(-\Delta G - \lambda - \epsilon)^2}{4\lambda k_B T}\right] \quad (47)$$

where

$$W = \frac{2\pi}{\hbar}\frac{\langle T_{DA}{}^2\rangle}{\sqrt{4\pi\lambda k_B T}} \quad (48)$$

$$C = \frac{\langle T_{DA}\rangle^2}{\langle T_{DA}{}^2\rangle} \quad (49)$$

$$\gamma = \frac{1}{\tau_c} \quad (50)$$

where C is the same as the coherence parameter defined by Balabin and Onuchic.[13] The empirical formula of eq 47 is quite useful to investigate the non-Condon effect on the ET rate because it involves only one kind of integral which is easily done numerically. Using eq 47, we investigate the τ_c dependence of $k_{DA}(-\Delta G)$. We choose the parameter value as follows:

$$\lambda = 0.60 \text{ eV}, \quad W = 1.94 \times 10^9 \text{ s}^{-1}, \quad C = 0.405, \quad T = 300 \text{ K} \quad (51)$$

In Figure 11A, we show the calculated curves of $k_{DA}(-\Delta G)$ by colored lines for $\tau_c = 4$, 15, 60, 250, and 1000 fs, respectively. We find that the normal region and the maximum region are not largely affected by the values of τ_c except for $\tau_c = 4$ fs. In the case of $\tau_c = 4$ fs, the normal region and the peak region are shifted a little to the larger energy gap side. We find that the five curves in the anomalous inverted region are parallel among them. We also find that the level of the anomalous inverted region is increased by 4 times, as τ_c is decreased by 4 times. Namely, the level of the slowly decreasing curve is proportional to $1/\tau_c$.

For the purpose of comparing the present calculations with the previous theoretical results later, we calculate $k_{DA}(-\Delta G)$ for the uncommon parameter values of τ_c. The results are plotted in Figure 11A by black lines for (1) 100 ps, (2) 10 ps, (3) 1 fs, (4) 100 as, and (5) 10 as.

To observe the τ_c dependence of the energy gap law in the normal region, we conducted the similar calculations to the above using $\lambda = 0.10$ eV and the same parameter values in eq 51 other than λ. The calculated result is plotted in Figure 11B by the colored lines for $\tau_c = 4$, 15, 60, 250, and 1000 fs, respectively. We observe the similar result to Figure 11A for the inverted region and around the maximum region of the energy gap law, although the position of the maximum k_{DA} is shifted to the larger energy gap by about 0.10 eV. In the normal region, we clearly see that k_{DA} is substantially elevated for the energy gap $-\Delta G < -0.2$ eV as τ_c becomes small. We also calculated $k_{DA}(-\Delta G)$ for the uncommon parameter values of τ_c. The results are plotted in Figure 11B by black lines.

Let us compare the present results with the previous theoretical works. Tang[23] approximately solved the Liouville equation for the density operator by adopting the spin-boson model

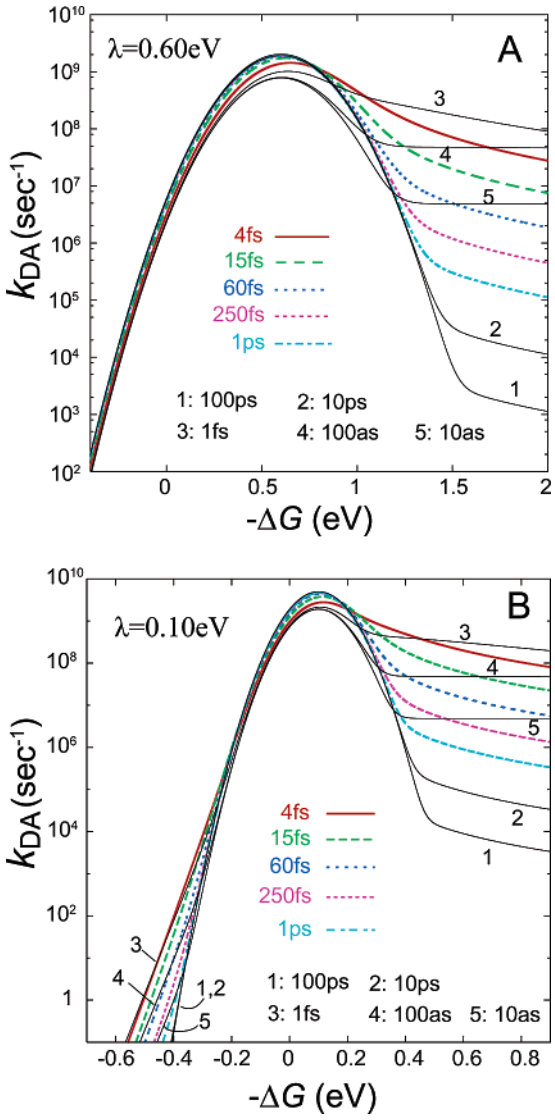

Figure 11. Correlation time τ_c dependence of the energy gap law. (A) Energy gap law with $\lambda = 0.60$ eV. The colored lines are for $\tau_c =$ 4, 15, 60 250, 1000 fs, respectively. The black lines are (1) 100 ps, (2) 10 ps, (3) 1 fs, (4) 100 as, and (5) 10 as. (B) Energy gap law with $\lambda = 0.10$ eV. The others are the same as in A.

Hamiltonian and the exponential form of the autocorrelation function of T_{DA} with the condition $\langle T_{DA}\rangle = 0$. Goychuk et al.[24] also approximately solved the Liouville equation by adopting the dichotomically fluctuating tunneling coupling model and the exponential form of the autocorrelation function with a condition $\langle T_{DA}\rangle \neq 0$. Tang obtained a result that the energy gap law is identical to the Marcus expression in the range of long correlation time τ_c. In the intermediate range of τ_c, the rate in the inverted region is increased rapidly with the decrease of τ_c, goes to the maximum, and then decreases with decrease of τ_c.[23] Goychuk et al. obtained a similar result to Tang. However, one more step is added: The rate decreases with the increase of τ_c in the limit of large τ_c due to the adoption of the dichotoic fluctuation model.[24] Our results of the τ_c dependence of k_{DA} in the anomalous inverted region are shown in Figure 11A. When the value of τ_c is decreased from such as 100 ps to 10 as for a fixed value of $-\Delta G$ (for example $-\Delta G = 1.5$ eV), k_{DA} increases for 1 fs $< \tau_c <$ 100 ps and turns to a decrease for $\tau_c < 1$ fs. When the value of τ_c is increased from 100 ps, it is evident that the value of k_{DA} remains constant since the curve is almost merged in the parabola at $\tau_c = 100$ ps. Since the

parameter values adopted by Tang are arbitrarily chosen and are different from ours, the τ_c values of the turning points of the k_{DA} value of Tang[23] does not correspond to ours. However, qualitative features of the τ_c dependence of k_{DA} in the inverted region agree with our results. Similarly, the results of Goychuk et al.[24] also qualitatively agree with ours except for the property that k_{DA} decreases with the increase of τ_c in the limit of large τ_c.

None of the previous theoretical works of the non-Condon effect on the ET suggested the anomalous normal region correctly. This is because the detailed balance condition which is indispensable for the presence of the anomalous normal region was not satisfied in the previous theories. Our results of the τ_c dependence of the energy gap law for $\lambda = 0.10$ eV are shown in Figure 11B. When the value of τ_c is decreased from 10 ps to 10 as for a fixed value of $-\Delta G$ (for example $-\Delta G = -0.4$ eV), k_{DA} increases for 4 fs $< \tau_c <$ 10 ps and turns to decrease for $\tau_c <$ 4 fs. When the value of τ_c is increased from 10 ps, the value of k_{DA} remains constant, since the curve is already merged in the parabola at $\tau_c = 10$ ps.

Next, we compare our results with those of Stuchebrukhov et al.[11,25,52,53] They first observed that there exist components of oscillation with a period of almost 20−30 fs (probably due to high-frequency vibrational modes) in the fluctuation of T_{DA} obtained by the MD simulation calculation.[11] On the basis of this result, they introduced an additional correlation function $F_1(t)$ corresponding to a high-frequency vibrational mode in the rate equation (eq 3.10 in ref 11). This $F_1(t)$ would correspond to the Fourier transform of our $P(\epsilon)$. By assuming an analytical form for $F_1(t)$, they derived a formula of k_{DA} including the non-Condon effect due to the high-frequency vibrational mode. They obtained a result that the maximum of the energy gap law is shifted to the larger energy side and the width of the energy gap law becomes broader as the contribution of the high-frequency vibrational mode becomes large. These results are quite different from ours in Figure 11. The origin of the discrepancy between the two results is the different forms of $F_1(t)$ and the Fourier transform of $P(\epsilon)$. Indeed, we observed remarkable oscillation of $T_{DA}(t)$ with a period of 20−30 fs of high-frequency vibrations as shown in the *inset* of Figure 2. However, the effect of the high-frequency vibrations to $P(\epsilon)$ is small as shown by the small peaks at around 1300 and 1700 cm^{-1} in Figure 4. The most important property in $P(\epsilon)$ is the long tail which extends over more than 8000 cm^{-1}. This long tail comes from the exponential decrease of the autocorrelation function $A(t)$ in Figure 3. From our analysis, we can say that the contribution of the high-frequency vibrations to the non-Condon effect is not as large as that expected by Stuchebrukhov et al.[11,25,52,53] at least in our system.

The above results of the τ_c dependence of the energy gap law indicate that if we can adjust the value of τ_c, we can regulate the ET rate in the anomalous energy gap region. The non-Condon effect which produces the anomalous energy gap law can become the third factor to regulate the ET rate in addition to the two factors: donor−acceptor distance and the energy gap. In that case, there is the important question by what method τ_c can be changed. To consider this problem, we should investigate how much τ_c differs among protein environments, polar solutions, and gas phases.

5.5. Experimental Evidence for the Anomalous Inverted Region. Some experimental data of the energy gap law have remained as unsolved problems until now. One such problem is the energy gap law of the quenching rate k_q of fluorescer molecules by quencher molecules in polar solution provided by Rehm and Weller in 1970.[54] This fluorescence quenching takes place due to the ET between the excited state of fluorescer and quencher. It is believed that this ET takes place after forming the encounter complex by the diffusion motion on each other. The experimental data showed that k_q does not decline below the diffusion limit rate until $-\Delta G = 2.6$ eV, where the inverted region of the Marcus' parabola already declines much below the diffusion limit rate (See Figure 12). To explain this anomalous behavior in the inverted region, at first it was proposed that a possible nonlinear effect in the dielectric response of polar solvent around ionic species can enhance the value of k_q at the large energy gap and that this nonlinear effect can be a candidate to explain the anomalous inverted region of the experiment by Rehm and Weller.[37,55−58] However, it was found by the examination of charge transfer (CT) spectra[59] and by the MD simulation study[60−62] that the nonlinear effect is not so large as to explain the anomalous inverted region.

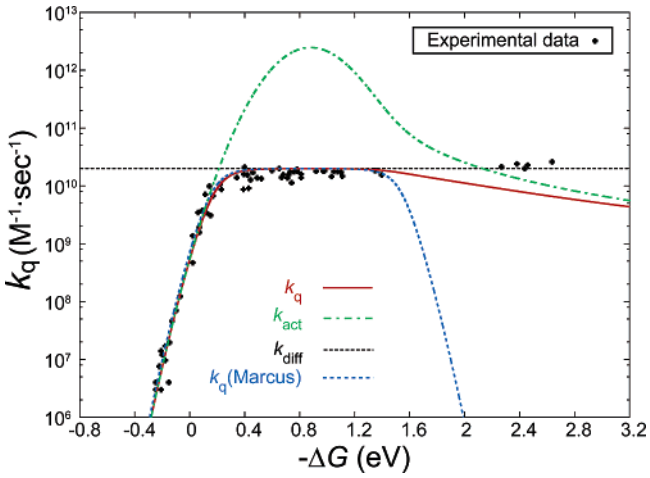

Figure 12. Comparison of theoretical and experimental energy gap laws of the fluorescence quenching rate constant k_q. The plus symbols represent the experimental data by Rehm and Weller.[54] The red curve is the theoretical curve of k_q obtained by considering the non-Condon effect in this paper. The green curve is the theoretical curve of k_{DA} with the non-Condon effect in this paper. The blue line represents the theoretical k_q calculated using k_{DA}^{el} equivalent to Marcus' parabola. The black line represents the diffusion limit rate constant.

Second, it was considered that there will be a distance distribution for the so-called collision complex. In general, the reorganization energy λ becomes large for the larger distance. Therefore, it was expected that the presence of the distance distribution will contribute to deform the Marcus parabola extending the width of the total energy gap law and that the inverted region will shift considerably to the larger energy gap.[63] The high frequency (quantum) vibrations also contribute to partly cease the rapid decrease of the rate in the inverted region.[64−66] The numerical calculations showed that the inverted region is actually shifted to the larger energy gap but that these effects alone were not enough to explain the total of the energy gap law of Rehm and Weller,[63,67−69] in which the normal region is located at the very small energy gap and no trace of the inverted region is seen in k_q until $-\Delta G = 2.6$ eV.[54]

Under these situations, the non-Condon effect in the present study which produces the anomalously long tail in the inverted region is promising to explain the experimental data of Rehm and Weller. In the following, we calculate k_q as a function of $-\Delta G$ by considering the non-Condon effect, but not considering the distance-distribution effect. The fluorescence quenching rate constant k_q is written by[70]

$$\frac{1}{k_q} = \frac{1}{k_{act}} + \frac{1}{k_{diff}} \tag{52}$$

where k_{act} is the second-order rate constant of ET and k_{diff} is the diffusion rate constant. This k_{act} is related to k_{DA} by the relation[71]

$$k_{act} = \frac{4\pi {R_0}^2 \Delta R N_A}{1000} k_{DA} \tag{53}$$

where R_0 is the average donor−acceptor distance at the encounter complex, ΔR is the distribution width of the encounter complex, and N_A is the Avogadro number.

We use eq 47 for k_{DA} and choose the parameter values as follows:

$$W = 10^{13}\ \mathrm{s}^{-1},\quad C = 0.5,\quad \tau_c = 10\ \mathrm{fs},\quad R_0 = 6\ \text{Å},$$
$$\lambda = 0.85\ \mathrm{eV},\quad T = 300\ \mathrm{K},\quad k_{diff} = 2 \times 10^{10}\ \mathrm{M}^{-1}\ \mathrm{s}^{-1},$$
$$\Delta R = 1\ \text{Å} \tag{54}$$

The calculated result is plotted in Figure 12. We find that the theoretical curve of k_q (red curve) fits the experimental data (plus symbol) very well except for a small discrepancy at the largest energy gap region 2.1−2.6 eV. The agreement is complete in the normal region. The Marcus parabola which corresponds to k_{DA}^{el} in our theory declines rapidly for $-\Delta G >$ 1.6 eV. We can say that almost all the properties of the energy gap law of Rehm and Weller can be well reproduced by the non-Condon theory. It is evident that the small discrepancy at the largest energy gap region around $-\Delta G = 2.4$ eV can be erased if we consider the distance distribution of the encounter complex and the effect of high-frequency (quantum) vibrations altogether. This detailed work is made elsewhere.

As a second example, we consider the energy gap law of the ET rate for Ru-modified cytochromes obtained by Mines et al.[72] The filled circles in Figure 13 are the experimental data. The broken lines represent the energy gap law of Marcus' parabola. The experimental points at the energy gap larger than 1.4 eV deviate largely upward from the Marcus parabola. Mines et al. suggested one possibility to explain this anomalous inverted region as follows:[72] The data points correspond to the ET values $^*Ru^{2+} \rightarrow Fe^{3+}$ and $Ru^{+} \rightarrow Fe^{3+}$. Formerly, it was suggested that there exists the triplet metal to ligand charge transfer (^{3}-MLCT) of $Fe(bpy)_3^{2+}$ at energy level 1.05 eV higher than the ground state.[73] Therefore, this excited state of Fe^{2+} in cytochrome can be the first acceptor state of the above ET. In such a case, the energy gaps for these reaction are reduced by 1.05 eV, and if the experimental energy gap law is shifted to the smaller energy gap points by 1.05 eV, they come to fit the Marcus' parabola. However, it should be noted that the electronic coupling will be reduced to some extent because the spin flip must happen in this ET.

Medvedev and Stuchebrukhov suggested another possibility to explain the anomalous inverted region by introducing the non-Condon effect due to the quantum vibration.[25] By adopting a large value of the non-Condon coupling parameter κL, they produced a broad energy gap law which passes well the experimental points of the inverted region.

In the following, we try to reproduce the anomalous inverted region in these systems by the non-Condon theory of eq 47. We choose the parameter values as follows:

$$W = 5.5 \times 10^{6}\ \mathrm{s}^{-1},\quad C = 0.40,\quad \tau_c = 6\ \mathrm{fs},\quad \lambda = 0.74\ \mathrm{eV},$$
$$T = 300\ \mathrm{K} \tag{55}$$

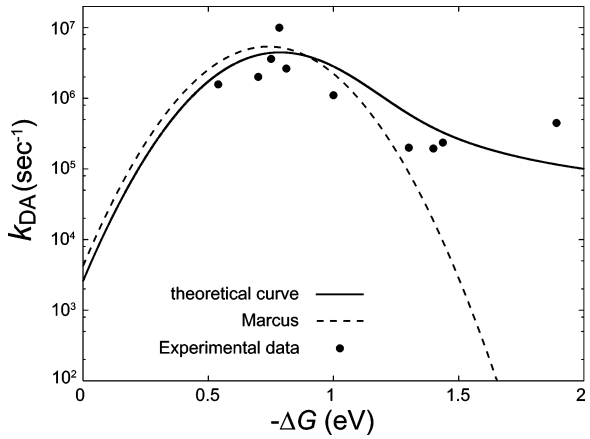

Figure 13. Comparison of theoretical and experimental energy gap laws in the ET of Ru-modified cytochromes. The filled circles are the experimental data.[72] The solid line represents the theoretical energy gap law calculated using k_{DA} with the non-Condon effect in this paper. The broken line represents the theoretical energy gap law calculated using k_{DA}^{el} equivalent to Marcus' parabola.

The calculated results are plotted by the solid line in Figure 13. The normal region and the maximum of the solid curve are shifted a little from the Marcus parabola due to a choice of a small value of τ_c. The inverted region locates at the high level and passes rather well the experimental points. The problem would be whether the correlation time τ_c can be as small as 6 fs, which must be examined in the future.

5.6. Physical Indication of the Fluctuating $T_{DA}(t)$. In the present paper, we clarified that $T_{DA}(t)$ has the following properties: (1) The number of occasions for the value of T_{DA} is almost described by the normal distribution function (Figure 9). (2) The essential part of the normalized autocorrelation function $A(t)$ of $T_{DA}(t)$ in the early time region which contributes to the overall property of $P(\epsilon)$ is expressed by an exponentially decreasing function. The property (1) just urges that the central limit theorem holds true in the stochastic sense. In order for the central limit theorem to apply, T_{DA} should be expressed as a sum of many independently fluctuating elements.[74] Here, let us be reminded of the fact that T_{DA} is expressed as[47,48]

$$T_{DA} = \hbar \sum_{a \in \Omega_D} \sum_{b \notin \Omega_D} J_{ab} \tag{56}$$

where Ω_D is a donor region separated by an arbitrary plane A inserted between donor and acceptor. J_{ab} is the interatomic tunneling current passing through the plane A. Equation 56 indicates that T_{DA} is formed by the sum of all the interatomic tunneling currents passing through plane A. Therefore, each interatomic tunneling current can be the fluctuating element in the normal distribution of T_{DA}. Since the plane A can be arbitrarily chosen, all the interatomic tunneling currents fluctuate almost independently. When the electron tunneling pathways are formed by connecting such interatomic tunneling currents, the mesh of the electron tunneling pathways must have a fully dynamic character. Indeed, we already observed that main tunneling routes fluctuate among the Trp route, Met route, and both routes.[18] The method of representing this dynamical character of the tunneling pathways more clearly should be developed in future.

Next we consider the physical meaning of the property (2) that the essential part of $A(t)$ can be approximately described by an exponentially decreasing function even though the role of quantum vibrations is not completely negligible. The exponentially decreasing function of $A(t)$ indicates that the

fluctuating dynamics of T_{DA} is based on the dissipative nuclear motions. The inset of Figure 3 shows that the downward concave curve in the early time region changes to the exponential curve at about 8 fs. This result indicates that the coherent dynamics of nuclear motions is destroyed within as short as 8 fs. Therefore, the time evolution of this system is mostly described as a Markovian process.[51] This characterization of the fluctuating property of $T_{DA}(t)$ will be useful for indentifying the mechanism of the long-range ET. Here, we should be reminded of the early theoretical work by Onuchic et al. on the validity of the Born−Oppenheimer approximation:[75] By adopting a model that one mode of vibration couples with the tunneling electron, they proved that the bridge part of the exact electronic state in the initial state is largely deviated from that of the initial electronic state of the Born−Oppenheimer approximation by the coherent nuclear motion. Then, they suggested that the Born−Oppenheimer approximation is bad for the long-distance ET by the superexchange mechanism. In this case, the coherent nuclear motion is assumed to be maintained for a long time (many periods of vibration). However, it is not evident whether the similar drawback of the Born−Oppenheimer approximation happens when many dissipative vibrational modes take part in the coupling with the tunneling electron, in which the overall coherent nuclear motions continue for a very small time (ca. less than 8 fs) as shown in the present study. This can be a problem for future work.

6. Conclusion

In this paper, we presented a new theory for the ET rate incorporating the non-Condon effect as correctly as possible. This theory satisfies the detailed balance condition for the forward and backward ET rates. We presented a recipe by which the decoupling of the tunneling mechanism into the elastic and inelastic ones is made with a mathematical principle. The dynamic property of the non-Condon effect is represented in the inelastic mechanism. The ET rate due to the elastic mechanism corresponds to the so-called ET rate in the slow modulation limit.

Sampling the $T_{DA}(t)$ data by conducting MD simulations and QC calculations for the ET of $Bph^- \rightarrow Q_A$ in the reaction center of *Rhodobacter sphaerides*, we obtained the time-correlation function $\langle T_{DA}(t)T_{DA}(0)\rangle_T$ and the normalized autocorrelation function $A(t)$. Performing the Fourier transform of $A(t)$ and making quantum correction, we obtained a reasonable power spectrum $P(\epsilon)$. We found that the essential part of $A(t)$ is expressed by an exponential form and the power spectrum has the long tail up to more than 8000 cm^{-1}. The ET rate is obtained by the convolution of $P(\epsilon)$ and the Franck−Condon factor. The non-Condon effect due to the inelastic mechanism had a dramatic effect on the energy gap law at the large energy gap in the inverted region and at the large uphill energy gap in the normal region.

We calculated the ratio of rates due to the inelastic and elastic mechanisms. As a result, we found that the energy gap dependence of the ratio is symmetrical with respect to $-\Delta G = 0$. The ratio is negative in the range $-a\lambda < -\Delta G < a\lambda$ where a is a factor close to 1, while the ratio is positive in the range $|-\Delta G| > a\lambda$. We found that this ratio increases very rapidly for $|-\Delta G| > 2a\lambda$. The anomalous energy gap law (anomalous inverted region and anomalous normal region) is due to the long tail of $P(\epsilon)$ due to the inelastic tunneling mechanism.

We presented experimental evidence for the anomalous inverted region, including the energy gap law of the fluorescence quenching rate in polar solution observed by Rehm and Weller.

We provided an empirical formula (eq 47) by which one can easily calculate the non-Condon ET rate. Using this formula, we calculated the τ_c dependence of the energy gap law. We found that the level of the anomalous inverted region is changed inversely in proportion to the correlation time τ_c of $A(t)$ for a reasonable range of τ_c values. Therefore, we propose that the modulation of the anomalous inverted region by τ_c should be used as the third method to regulate the ET rate in addition to the two methods: energy gap and donor−acceptor distance.

By performing the population analysis of the value of T_{DA}, we observed that it almost follows the normal distribution. From this result, we find that all the interatomic tunneling currents fluctuate almost independently. It holds true from the time scale of tens of femtoseconds since the autocorrelation function decays almost exponentially with a time constant of about 60 fs. Therefore, we conclude that the electron tunneling pathways, which are formed by connecting the interatomic tunneling currents, have a property of fully dynamical character.

Acknowledgment. This work was supported by the Grant-in-Aid on Scientific Research (C) to T.K. from the Ministry of Education, Culture, Sports, Science and Technology of Japan. This work was also supported by Grants-in-Aid for the 21st Century COE Program "Frontiers of Computational Science", and for the Scientific Research on the priority area "Genome Information Science" from the Ministry of Education, Culture, Sports, Science and Technology of Japan, and a Grants-in-Aid from the Hori Information Science Promotion Foundation to T.Y.

Appendix A

We prove that the non-Condon ET rate of eq 33 satisfies the detailed balance condition (eq 19).

From eq 34

$$k_{DA}^{el}(-\Delta G) = C_1 \exp\left[-\frac{(-\Delta G-\lambda)^2}{4\lambda k_B T}\right] = C_1 \times \exp\left[-\frac{(\Delta G-\lambda)^2}{4\lambda k_B T}\right]\cdot\exp\left[-\frac{\Delta G}{k_B T}\right] = k_{AD}^{el}(\Delta G)\exp\left[-\frac{\Delta G}{k_B T}\right] \quad \text{(A1)}$$

Equation A1 satisfies the detailed balance condition for k_{DA}^{el}.

From eq 35

$$k_{DA}^{inel}(-\Delta G) = C_2 \int_{-\infty}^{\infty} d\epsilon \int_{-\infty}^{\infty} dt\,(A(t)-1)\times \exp(i\epsilon t/\hbar)\frac{2}{1+\exp(-\epsilon/k_B T)}\exp\left[-\frac{(-\Delta G-\lambda-\epsilon)^2}{4\lambda k_B T}\right] = C_2 \int_{-\infty}^{\infty} d\epsilon \int_{-\infty}^{\infty} dt\,(A(t)-1)\exp (i\epsilon t/\hbar)\frac{2}{1+\exp(-\epsilon/k_B T)}\exp\left[-\frac{(\Delta G-\lambda-\epsilon)^2}{4\lambda k_B T}\right]\times \exp\left[-\frac{\Delta G(\lambda+\epsilon)}{\lambda k_B T}\right] \quad \text{(A2)}$$

Replacing $\epsilon \rightarrow -\epsilon'$ and $t \rightarrow -t'$, and using a property $A(t) = A(-t') = A(t')$, we obtain

$$k_{DA}^{inel}(-\Delta G) = C_2 \exp\left[-\frac{\Delta G}{k_B T}\right] \int_{-\infty}^{\infty} d\epsilon' \int_{-\infty}^{\infty} dt' \,(A(t') - 1) \exp(i\epsilon' t'/\hbar) \frac{2}{1+\exp(-\epsilon'/k_B T)} \times \exp\left[-\frac{(\Delta G - \lambda + \epsilon')^2}{4\lambda k_B T}\right] \exp\left[\frac{\Delta G \epsilon'}{\lambda k_B T}\right] = C_2 \times \exp\left[-\frac{\Delta G}{k_B T}\right] \int_{-\infty}^{\infty} d\epsilon' \int_{-\infty}^{\infty} dt' \,(A(t') - 1) \exp(i\epsilon' t'/\hbar) \frac{2}{1+\exp(-\epsilon'/k_B T)} \exp\left[-\frac{(\Delta G - \lambda - \epsilon')^2}{4\lambda k_B T}\right] = k_{AD}^{inel}(\Delta G) \exp\left[-\frac{\Delta G}{k_B T}\right] \quad \text{(A3)}$$

Equation A3 satisfies the detailed balance condition for k_{DA}^{inel}. Substituting eqs A1 and A3 into eq 33, we obtain

$$k_{DA}(-\Delta G) = k_{AD}(\Delta G) \exp\left[-\frac{\Delta G}{k_B T}\right] \quad \text{(A4)}$$

Equation A4 satisfies the detailed balance condition (eq 19) for k_{DA}.

It is straightforward to prove that the detailed balance condition is satisfied even when one uses a more general expression for the Franck−Condon factor as in eq 25, by the method similar to the previous study.[57]

Appendix B

We prove that $\sqrt{\langle T_{DA}{}^2 \rangle}$ is smaller than $|T_{DA}^i|$, which gives the maximum of B_i in Figure 10. We adopt a continuous valuable x instead of a discrete variable T_{DA}^i. We adopt a normal distribution function for simplicity as follows

$$f(x) = \frac{1}{\sqrt{2\pi}\sigma} \exp\left[-\frac{(x - x_0)^2}{2\sigma^2}\right] \quad \text{(B1)}$$

where x_0 is a constant and σ^2 is the dispersion defined by

$$\sigma^2 = \int_{-\infty}^{\infty} (x - x_0)^2 f(x)\, dx \quad \text{(B2)}$$

The participation ratio B_i is replaced by

$$g(x) = \frac{x^2 f(x)}{\int_{-\infty}^{\infty} x^2 f(x)\, dx} \equiv \frac{x^2 f(x)}{\langle x^2 \rangle} \quad \text{(B3)}$$

We easily obtain

$$\langle x^2 \rangle = \sigma^2 + x_0{}^2 \quad \text{(B4)}$$

We obtain x_{max} which gives the maximum of $g(x)$ from the condition $dg(x)/dx = 0$

$$x_{max} = \frac{1}{2}(x_0 + \sqrt{x_0{}^2 + 8\sigma^2}) \quad \text{(B5)}$$

where we adopted only a positive value of x. From eqs B4 and B5

$$x_{max}{}^2 - \langle x^2 \rangle = \frac{1}{2} x_0{}^2 (\sqrt{1 + 8\sigma^2/x_0{}^2} - 1) + \sigma^2 > 0 \quad \text{(B6)}$$

Therefore, we proved

$$x_{max} > \sqrt{\langle x^2 \rangle} \quad \text{(B7)}$$

References and Notes

(1) Marcus, R. A.; Sutin, N. *Biochim. Biophys. Acta* **1985**, *811*, 265.
(2) Moser, C. C.; Keske, J. M.; Warnucke, K.; Farid, R. S.; Dutton, P. L. *Nature* **1992**, *355*, 796.
(3) McCornell, H. M. *J. Chem. Phys.* **1961**, *35*, 508.
(4) Beratan, D. N.; Onuchic, J. N.; Hopfield, J. J. *J. Chem. Phys.* **1987**, *86*, 4488.
(5) Onuchic, J. N.; Beratan, D. N.; Winkler, J. R.; Gray, H. B. *Annu. Rev. Biophys. Biomol. Struct.* **1992**, *21*, 349.
(6) Regan, J. J.; Bilio, A. J. D.; Langen, R.; Skov, L. K.; Winkler, J. R.; Gray, H. B.; Onuchic, J. N. *Chem. Biol.* **1995**, *2*, 489.
(7) de Andrade, P. C. P.; Onuchic, J. N. *J. Chem. Phys.* **1998**, *108*, 4249.
(8) Wuttke, D. S.; Bjerrum, J. H.; Winkler, J. R.; Gray, H. B. *Science* **1992**, *256*, 1007.
(9) Curry, W. B.; Grabe, M. D.; Kurnikov, I. V.; Skourtis, S. S.; Beratan, D. N.; Regan, J. J.; Aquino, A. J. A.; Beroza, P.; Onuchic, J. N. *J. Bioenerg. Biomembr.* **1995**, *27*, 285.
(10) Kestner, N.; Logan, J. Jortner, J. *J. Phys. Chem.* **1974**, *78*, 2148.
(11) Daizadeh, I.; Medvedev, E. S.; Stuchebrukhov, A. A. *Proc. Natl. Acad. Sci. U.S.A.* **1997**, *94*, 3703.
(12) Antony, J.; Medvedev, D. M.; Stuchebrukhov, A. A. *J. Am. Chem. Soc.* **2000**, *122*, 1057.
(13) Balabin, I. A.; Onuchic, J. N. *Science* **2000**, *290*, 114.
(14) Xie, Q.; Archontis, G.; Skourtis, S. S. *Chem. Phys. Lett.* **1997**, *312*, 237.
(15) Kawatsu, T.; Kakitani, T.; Yamato, T. *J. Phys. Chem. B* **2002**, *106*, 11356.
(16) Kobayashi, C.; Baldridge, K.; Onuchic, J. N. *J. Chem. Phys.* **2003**, *119*, 3550.
(17) Tan, M.-L.; Balabin, I. A.; Onuchic, J. N. *Biophys. J.* **2004**, *86*, 1813.
(18) Nishioka, H.; Kimura, A.; Yamato, T.; Kawatsu, T.; Kakitani, T. *J. Phys. Chem. B* **2005**, *109*, 1978.
(19) Skourtis, S. S.; Balabin, I. A.; Kawatsu, T.; Beratan, D. N. *Proc. Natl. Acad. Sci. U. S. A.* **2005**, *102*, 3552.
(20) Prytkova, T. R.; Kurnikov, I. V.; Beratan, D. N. *J. Phys. Chem. B* **2005**, *109*, 1618.
(21) Ratner, M. A. *Proc. Natl. Acad. Sci. U. S. A.* **2001**, *98*, 387.
(22) Berlin, Y. A.; Burin, A. L.; Siebbeles, L. D. A.; Ratner, M. A. *J. Phys. Chem. A* **2001**, *105*, 5666.
(23) Tang, J. *J. Chem. Phys.* **1993**, *98*, 6263.
(24) Goychuk, I. A.; Petrov, E. G.; May, V. *J. Chem. Phys.* **1995**, *103*, 4937.
(25) Medvedev, E. S.; Stuchebrukhov, A. A. *J. Chem. Phys.* **1997**, *107*, 3821.
(26) Bixon, M.; Jortner, J. *Russ. J. Electrochem.* **2003**, *39*, 3.
(27) Troisi, A.; Nitzan, A.; Ratner, M. A. *J. Chem. Phys.* **2003**, *119*, 5782.
(28) Troisi, A.; Ratner, M. A.; Zimmt, M. B. *J. Am. Chem. Soc.* **2004**, *126*, 2215.
(29) Neria, E.; Nitzan, A.; Barnett, R. N.; Landman, U. *Phys. Rev. Lett.* **1991**, *67*, 1011.
(30) Neria, E.; Nitzan, A. *J. Chem. Phys.* **1993**, *99*, 1109.
(31) Schwartz, B. J.; Bittner, E. R.; Prezhdo O. V.; Rossky, P. J. *J. Chem. Phys.* **1996**, *104*, 5942.
(32) Prezhdo O. V.; Rossky, P. J. *J. Chem. Phys.* **1997**, *107*, 5863.
(33) Heller, E. J. *J. Chem. Phys.* **1975**, *62*, 1544.
(34) Heller, E. J. *J. Chem. Phys.* **1976**, *64*, 63.
(35) Heller, E. J. *J. Chem. Phys.* **1981**, *75*, 2923.
(36) Oxtoby, D. W. *Adv. Chem. Phys.* **1981**, *47*, 487.
(37) Kakitani, T.; Mataga, N.. *Chem. Phys.* **1985**, *93*, 381.
(38) Stowell, M. H. B.; McPhillips, T. M.; Rees, D. C.; Soltis S. M.; Abresch, E.; Feher G. *Science* **1997**, *276*, 812.
(39) Morikami, K.; Nakai, T.; Kidera, A.; Saito, M.; Nakamura, H. *Comput. Chem.* **1992**, *16*, 243. PRESTO (A vectorized molecular mechanics program for biopolymers).
(40) Cornell, W. D.; Cieplak, P.; Bayly, C. I.; Gould, I. R.; Merz, K. M., Jr.; Ferguson, D. M.; Spellmeyer, D. C.; Fox, T.; Caldwell, J. W.; Kollman, P. A. *J. Am. Chem. Soc.* **1995**, *117*, 5179.
(41) Saito, M. *Mol. Simul.* **1992**, *8*, 321.
(42) Ryckaert, J. P.; Ciccotti, G.; Berendsen, H. J. C. *J. Comput. Phys.* **1977**, *23*, 327.
(43) Howell, J.; Rossi, A.; Wallace, D.; Haraki, K.; Hoffmann, R. *QCPE* **1977**, *11*, 344. FORTICON8 (Extended Hückel method program).

(44) Kincaid, D. R.; Respess, J. R.; Young, D. M.; Grimes, R. G. *ITPACK 2C*; University of Texas: Austin, TX, 1999 (a Fortran package for solving large sparse linear systems by adaptive accelerated iterative methods).
(45) Stewart, J. J. P. *J. Comput. Chem.* **1989**, *10*, 209.
(46) Frisch, M. J.; Trucks, G. W.; Schlegel, H. B.; Scuseria, G. E.; Robb, M. A.; Cheeseman, J.R.; Zakrzewski, V. G.; Montgomery, J. A., Jr.; Stratmann, R. E.; Burant, J. C.; Dapprich, S.; Millam, J. M.; Daniels, A. D.; Kudin, K. N.; Strain, M. C.; Farkas, O.; Tomasi, J.; Barone, V.; Cossi, M.; Cammi, R.; Mennucci, B.; Pomelli, C.; Adamo, C.; Clifford, S.; Ochterski, J.; Petersson, G. A.; Ayala, P. Y.; Cui, Q.; Morokuma, K.; Malick, D. K.; Rabuck, A. D.; Raghavachari, K.; Foresman, J. B.; Cioslowski, J.; Ortiz, J. V.; Baboul, A. G.; Stefanov, B. B.; Liu, G.; Liashenko, A.; Piskorz, P.; Komaromi, I.; Gomperts, R.; Martin, R. L.; Fox, D. J.; Keith, T.; Al-Laham, M. A.; Peng, C. Y.; Nanayakkara, A.; Challacombe, M.; Gill, P. M. W.; Johnson, B.; Chen, W.; Wong, M. W.; Andres, J. L.; Gonzalez, C.; Head-Gordon, M.; Replogle, E. S.; Pople, J. A. *Gaussian98*, revision A.9; Gaussian, Inc.: Pittsburgh, PA, 1998.
(47) Kawatsu, T.; Kakitani, T.; Yamato T. *Inorg. Chim. Acta* **2000**, *300*−*302*, 862.
(48) Kawatsu, T.; Kakitani, T.; Yamato T. *J. Phys. Chem. B* **2001**, *105*, 4424.
(49) Kawatsu, T.; Kakitani, T.; Yamato, T. *J. Phys. Chem. B* **2002**, *106*, 5068.
(50) Gunner, M. R..; Dutton, P. L. *J. Am. Chem. Soc.* **1989**, *111*, 3400.
(51) Kubo, R.; Toda, M.; Hashitsume, N. *Statistical Physics. II. Nonequilibrium Statistical Mechanics*, 2nd ed.; Springer: Heidelberg, 1995.
(52) Medvedev, E. S.; Stuchebrukhov, A. A. *Pure Appl. Chem.* **1998**, *70*, 2201.
(53) Medvedev, E. S.; Stuchebrukhov, A. A. *Chem. Phys.* **2004**, *296*, 181.
(54) Rehm, D.; Weller, A. *Isr. J. Chem.* **1970**, *8*, 259.
(55) Kakitani, T.; Mataga, N. *J. Phys. Chem.* **1985**, *89*, 8.
(56) Kakitani, T.; Mataga, N. *J. Phys. Chem.* **1986**, *90*, 993.
(57) Kakitani, T.; Mataga, N. *J. Phys. Chem.* **1987**, *91*, 6277.
(58) Yoshimori, A.; Kakitani, T.; Enomoto, Y.; Mataga, N. *J. Phys. Chem.* **1989**, *93*, 8316.
(59) Marcus, R. A. *J. Phys. Chem.* **1989**, *93*, 3078.
(60) Kuharski, R. A.; Bader, J. S.; Chandler, D.; Sprik, M.; Klein, M. L.; Impey, R. W. *J. Chem. Phys.* **1988**, *89*, 3248.
(61) Hwang, J.-K.; Warshel, A. *J. Am. Chem. Soc.* **1987**, *109*, 715.
(62) King, G.; Warshel, A. *J. Chem. Phys.* **1990**, *93*, 8682.
(63) Kakitani, T.; Yoshimori, A.; Mataga, N. *Electron Transfer in Inorganic, Organic and Biological Systems*; Bolton, J., et al., Eds.; Advances in Chemistry Series; American Chemical Society: Washington, DC, 1991; Chapter 4.
(64) Ulstrup, J.; Jortner, J. *J. Chem. Phys.* **1975**, *63*, 4358.
(65) Miller, J. R.; Calcaterra, L. T.; Closs, G. L. *J. Am. Chem. Soc.* **1984**, *106*, 3047.
(66) Closs, G. L.; Miller, J. R. *Science* **1988**, *240*, 440.
(67) Kakitani, T.; Yoshimori, A.; Mataga, N. *J. Phys. Chem.* **1992**, *96*, 5385.
(68) Tachiya, M.; Murata, S. *J. Phys. Chem.* **1992**, *96*, 8441.
(69) Kakitani, T.; Matsuda, N. Yoshimori, A.; Mataga, N. *Prog. React. Kinet.* **1995**, *20*, 347.
(70) Marcus, R. A.; Siders, P. *J. Phys. Chem.* **1982**, *86*, 622.
(71) Brunschwig, B. S.; Ehrenson, S.; Sutin, N. *J. Am. Chem. Soc.* **1984**, *106*, 6858.
(72) Mines, G. A.; Bjerrum, M. J.; Hill, M. G.; Casimiro, D. R.; Chang, I.-J.; Winkler, J. R.; Gray, H. B. *J. Am. Chem. Soc.* **1996**, *118*, 1961.
(73) Kober E. M.; Meyer, T. J. *Inorg. Chem.* **1982**, *21*, 3967.
(74) Stuchebrukhov, A. A. *J. Chem. Phys.* **1996**, *105*, 10819.
(75) Onuchic, J. N.; Beratan, D. N.; Hopfield, J. J. *J. Phys. Chem.* **1986**, *90*, 3707.